

A HUBBLE SPACE TELESCOPE SURVEY OF EXTENDED [OIII] λ 5007Å EMISSION IN A FAR-INFRARED SELECTED SAMPLE OF SEYFERT GALAXIES: OBSERVATIONS¹

H. R. SCHMITT^{2,3,4}, J. L. DONLEY^{5,6}, R. R. J. ANTONUCCI⁷, J. B. HUTCHINGS⁸, A. L. KINNEY⁹
To appear in The Astrophysical Journal Supplement Series October 2003 issue

ABSTRACT

We present a Hubble Space Telescope (HST) survey of extended [OIII] emission for a sample of 60 Seyfert galaxies (22 Seyfert 1's and 38 Seyfert 2's), selected based on their far infrared properties. The observations for 42 of these galaxies were done in a snapshot survey with WFPC2. The remaining 18 were obtained from the HST archive, most of which were observed with the same configuration. These observations cover 68% of the objects in the sample defined by Kinney et al. (2000), and create a valuable dataset for the study of the Narrow Line Region (NLR) properties of Seyfert galaxies. In this paper, we present the details of the observations, reductions, and measurements. We also discuss the extended structure of individual sources, and the relation of this emission to the radio and host galaxy morphology. We also address how representative the subsample of [O III]-imaged galaxies is of the entire sample, and possible selection effects that may affect this comparison of the properties of Seyfert 1 and Seyfert 2 galaxies.

Subject headings: galaxies:active – galaxies:Seyfert – galaxies:structure – galaxies:emission lines – galaxies:nuclei – surveys

1. INTRODUCTION

The Unified Model for Seyfert galaxies (Antonucci 1993; Urry & Padovani 1995) is based in part on the idea that the nuclear region of these galaxies is surrounded by a dusty torus. Under this scenario, the distinction between Seyfert 1's and Seyfert 2's depends on whether the nucleus is observed through the torus pole (Seyfert 1's) or equator (Seyfert 2's). Starting with the spectropolarimetric observations of NGC 1068 (Antonucci & Miller 1985) several tests have been applied to this model, which is now supported by several lines of evidence, and is widely accepted by the AGN community as broadly, if not universally, applicable.

Some of the most important evidence for this model are the observation of a deficit of ionizing photons in Seyfert 2 galaxies (Neugebauer et al. 1980; Wilson, Ward & Haniff 1988; Storchi-Bergmann, Wilson & Baldwin 1992), and the collimated escape of radiation from the nucleus. The collimated radiation is observed in the form of ionization cones, seen in the light of high ionization gas such as [OIII] λ 5007Å, or ionization maps created by dividing [OIII] images by H α + [NII] λ 6548,84Å ones (Pogge 1988a,b,1989; Haniff, Wilson & Ward 1988; Mulchaey, Wilson & Tsvetanov 1996a,b).

The most extensive study of the morphologies and sizes of the NLRs of Seyferts was done by Mulchaey et al. (1996a), using ground-based observations. However, due

to the fact that in most of these galaxies the emission is concentrated in the inner 2'' region around the nucleus, most of their sources revealed only halo-like [OIII] emission. Higher spatial resolution images, like those achievable with HST, are necessary for a detailed study of the NLR of these sources.

So far, however, most of the studies done using HST images (Schmitt & Kinney 1996; Capetti et al. 1996; Falcke, Wilson & Simpson 1998, Ferruit et al. 2000) involved small samples of galaxies, and probably suffered from major selection effects. In an attempt to solve this sample problem we performed an HST snapshot survey to observe the extended [OIII] emission in a large and well-defined sample of Seyfert galaxies. We consider it very important that our sample was selected to be as free as possible of orientation biases that invalidate comparisons between two populations posited to be similar except in orientation. Here we present the results of this snapshot survey, which obtained data for 42 galaxies, as well as similar data for another 18 Seyfert galaxies, obtained from the HST archive. We discuss the sample selection, observations, data reductions, and measurements. We also compare the distances and luminosities of the observed galaxies with those of the entire Kinney et al (2000) sample, to verify that they are a representative subsample, and can be used to draw robust statistics on the Unified Model. Similarly, we compare the distances, luminosities and limits of detection of extended

¹ Based on observations made with the NASA/ESA Hubble Space Telescope, which is operated by the Association of Universities for Research in Astronomy, Inc., under NASA contract NAS5-26555.

² National Radio Astronomy Observatory, 520 Edgemont Road, Charlottesville, VA22903.

³ Jansky Fellow.

⁴ email:hschmitt@nrao.edu

⁵ Department of Astronomy and Astrophysics, The Pennsylvania State University, 525 Davey Laboratory, University Park, PA16802

⁶ National Radio Astronomy Observatory, P.O. Box 0, Socorro, NM87801.

⁷ University of California, Santa Barbara, Physics Department, Santa Barbara, CA 93106.

⁸ Dominion Astrophysical Observatory, Herzberg Institute of Astrophysics, National Research Council of Canada, 5071 West Saanich Road, Victoria, BC V9E 2E7, Canada.

⁹ NASA Headquarters, 300 E Street SW, Washington, DC20546.

[OIII] emission of the observed Seyfert 1's to Seyfert 2's, to address possible selection effects.

Combining these [OIII] observations with the optical and radio ground-based observations that we have for this sample, we show that we have created a valuable dataset for the study of the Unified Model, the interaction between the radio and line emission in the NLR, and the ionization mechanisms for the gas. The comparison of the properties of the NLR's of Seyfert 1's and Seyfert 2's will be presented in a separate paper.

2. SAMPLE

One of the most important aspects of Unified Model studies is sample selection. During recent years, several papers have presented results which seem to contradict the model predictions, but most of these can be explained as due to selection effects (see Schmitt et al. 2001a; Ho & Ulvestad 2001 for a more detailed discussion). In order to test the Unified Model, one has to select a sample based on isotropic properties - those independent of the orientation of the torus to the line of sight. This will insure against selecting different types of Seyferts from different parts of the luminosity function (e.g. intrinsically brighter Seyfert 2's), or any other orientation-dependent biases.

In our recent work, we have used the sample of Seyfert galaxies extracted from the catalog of warm infrared sources of de Grijp et al. (1987, 1992), which were selected based on their $60\mu\text{m}$ luminosities and warm $25/60\mu\text{m}$ colors. Our sample, described in Kinney et al. (2000), includes all the Seyfert galaxies with $z < 0.031$ in this catalog, for a total of 88 sources (29 Seyfert 1's and 59 Seyfert 2's). Notice that Kinney et al. (2000) combined all Seyfert 1 and 1.5 galaxies in the Seyfert 1 group, and all the Seyfert 1.8, 1.9 and 2 in the Seyfert 2 group. We have made an extensive study of the properties of this sample (Schmitt et al. 2001a), which currently includes ground-based B and I images (Schmitt & Kinney 2000), and high resolution (3.6cm VLA) radio images (Schmitt et al. 2001b, S01b hereafter) for most of the galaxies.

3. OBSERVATIONS

All the observations presented in this paper are from HST. Most of these observations (45 of the 63 galaxies), are from snapshot proposal 8598 (P.I. Schmitt). Data for another 18 galaxies were available in the HST archive, observed for the following programs: 3982 (P.I. Baldwin), 5140 (P.I. Macchetto), 5745 (P.I. Ford), 6332, 6419, 8240 (P.I. Wilson) and 8259 (P.I. Whittle). Although some of the archival data have been presented elsewhere, we have re-reduced them to present here in a homogeneous manner, and as a check of the reduction process. Observations of 3 sources in our snapshot survey failed, so the total number of galaxies with [OIII] images is 60, which corresponds to $\approx 70\%$ of the full $60\mu\text{m}$ sample (22 Seyfert 1's and 38 Seyfert 2's). Of the three observations which failed, two were due to guide star acquisition problems (UGC 10683 B and IRAS 11215-2806), and one to the misfortune that the nucleus of the galaxy fell on bad CCD columns (Fairall 49).

The majority of the galaxies in the sample were observed with the WFPC2 camera. The exceptions are NGC 3393, which was observed with the WF/PC1 camera in PC mode (pre-COSTAR), and MRK 3, which was observed with the

FOC camera (post-COSTAR). Details on the reduction of these two sources are given in Schmitt & Kinney (1996). In the case of the galaxies observed with WFPC2, only 2 out of the 61 objects had radial velocities smaller than $\sim 1500 \text{ km s}^{-1}$ (NGC 1068 and NGC 1386) and consequently their on-band images were observed with the narrow band filter F502N in the PC camera. The remaining 59 galaxies had to be observed with the Linear Ramp Filter.

The WFPC2 Linear Ramp Filter has a strip where the central wavelength varies along the position, with a bandwidth of approximately 1.3% of the central wavelength ($\sim 65\text{\AA}$), so it can only be used to image sources smaller than $\sim 13''$. Previous ground-based observations (Mulchaey et al. 1996a,b) show that most Seyfert galaxies have NLR's with sizes smaller than $\sim 2''$, indicating that a $13''$ field of view is a good match for our project.

An important detail about observations with the Linear Ramp Filter is that the coordinates of the sources have to be known with an accuracy of $\sim 1''$ or better, to place them in the region of the filter which covers the wavelength of interest. We checked this by comparing the position where the source was expected to fall on the CCD (calculated using the redshifted wavelength of the [OIII] line, and the information in the HST Manual), with the observed position of the nucleus of the galaxy. None of the observations were missed because of pointing problems. Figure 1 presents the difference between the expected and observed positions of the galaxies. This Figure shows that in most of the cases the galaxy falls within $2''$ from the expected position, with the median distance being $1.12''$. These displacements from the expected position are consistent with the coordinate and pointing uncertainties. The most deviant point in the sample corresponds to NGC 4968, which falls at $6.63''$ from the expected position. This is mostly due to the uncertainty in the coordinates of the galaxy ($8''$). According to Pogge (1989), the ground based [OIII] image of this source shows only an unresolved point source, so the large shift from the expected position did not influence our results.

Another detail of the Linear Ramp Filter observations is the fact that, for those galaxies with radial velocity larger than $\sim 8600 \text{ km s}^{-1}$, the redshifted [OIII] $\lambda 5007\text{\AA}$ line no longer falls on the second WF camera chip, but actually on the PC camera. Although observations with the PC camera would in some sense be desirable, because of the smaller pixel size and better sampling, the sensitivity of this camera is significantly lower than that of the WF camera. This would require a much larger integration time to achieve sensitivities similar to the ones obtain with the WF camera, thus reducing the likelihood of the source being observed as a snapshot. In cases like this, we took into account the fact that the bandwidth of the Linear Ramp filter is 1.3% of the central wavelength ($\sim 4000 \text{ km s}^{-1}$) and forced the galaxies with radial velocities between 8600 km s^{-1} and 9100 km s^{-1} to fall on the second WF camera chip, at the position corresponding to [OIII] $\lambda 5007\text{\AA}$ redshifted by 8600 km s^{-1} . The only exception to this procedure is NGC 7674, which was extracted from the archive (project 8259). This galaxy was observed with the Linear Ramp filter on the PC camera.

The on-band observations of our snapshot survey had total exposure times between 600 and 1000 seconds, with

the stronger sources having shorter integrations and the fainter ones having longer integrations. The exposures were split into 2 integrations of same duration, to allow the easier elimination of cosmic rays. The observations taken from the archive were obtained with similar total exposure times, and were also split into 2 or more individual exposures.

In order to be able to subtract the host galaxy contribution to the on-band images, we obtained short exposure continuum images using the intermediate band filter F547M. This filter is in a line-free region of the spectrum, and the contribution from redshifted [OIII] emission is expected to be small, because in all cases this line falls at wavelengths where the transmission is less than 50% of that of the peak of the filter. Due to time constraints in our snapshot survey, we did not obtain multiple exposures with this filter, but only a single 80-second integration per galaxy. Most of the galaxies extracted from the archive also used this filter to obtain continuum images, but usually had multiple exposures. In the case of the project 6332, the continuum observations were also done with the Linear Ramp Filter, instead of F547M.

Table 1 presents a summary of the observations, where we give the names of the galaxies, their coordinates, exposure times, the names of the datasets in the HST archive, the proposal which observed the galaxy, and comments. Each entry in this Table is divided into 2 or 3 lines, with the first ones corresponding to the on-band observations, and the last one corresponding to the continuum observations.

4. REDUCTIONS AND MEASUREMENTS

The data reduction for the continuum images taken with filter F547M, and the on-band images taken with the filter F502N, followed the standard HST pipeline procedures. In the case of the observations taken with the Linear Ramp Filter, most of the reductions were done by the HST pipeline, with the exception of the flat field correction. Since there are no flat fields for this filter, we used the one for the filter F502N, which has a similar wavelength and bandwidth.

The on-band and continuum images were aligned using either a star in the same chip as the galaxy, or the nucleus of the galaxy when stars were not available. Multiple images were combined to eliminate cosmic rays. For those galaxies with only one continuum image, cosmic rays were first eliminated using an automatic routine, and the remaining ones eliminated by hand. All combined and cleaned on-band and continuum images were further inspected for cosmetic defects and cleaned.

Some extra care was necessary with the reduction of archive observations obtained by the project 6332, 8240 and 8259. Project 6332 used the Linear Ramp Filter to observe the continuum images, which resulted in the on-band and continuum images being located in different WF chips. A similar problem happened with the data taken from project 8240 and one of the galaxies observed by 8259 (NGC 4507), where the continuum observations were taken with the PC camera and the on-band images were taken with the WF camera. In these cases the four WFPC2 chips were first mosaiced, to correct for distortions and put the images on the same scale, and then aligned and combined

to eliminate cosmic rays.

The flux calibration of the continuum images taken with filter F547M, and the on-band images taken with filter F502N was done in the standard way, using the information available on the image headers. The calibration of the images taken with the Linear Ramp Filter was done with the WFPC2 Exposure Time Calculator for extended sources. For a source with a given flux, observed for a given exposure time at the redshifted [OIII] $\lambda 5007\text{\AA}$ wavelength, one is able to use the Exposure Time Calculator to determine its count rate and obtain a calibration coefficient. Based on these numbers, we estimate the photometric calibration for the different wavelengths observed has an accuracy of $\sim 5\%$.

The background for both on-band and continuum images was defined by averaging the mean counts in several regions around the galaxy. This value was subtracted from the corresponding images. Continuum free [OIII] images were created by subtracting a scaled continuum image from the on-band image. The scaling of the continuum images was estimated from the bandpass FWHM of the on-band filter. In some cases it was necessary to change this value by a small amount, to avoid over- or under-subtraction. Finally, we used emission free regions of the continuum-free [OIII] images to determine their r.m.s. (σ), clipped these images at 3σ above the background level and rotated them to put N up and E to the left.

The continuum-free [OIII] images were used to measure the [OIII] flux of these galaxies. We measured the nuclear fluxes, obtained using a circular aperture of a 100 parsecs in radius centered at the nucleus, and the total [OIII] fluxes, obtained integrating the flux inside a rectangular box placed around the regions of emission.

We present in Table 2 the names and alternate names of the galaxies, their Seyfert types, radial velocities, and the 3σ surface brightness detection limit of their [OIII] images, which also corresponds to the first contour level of the Figures. This Table also presents the [OIII] fluxes obtained integrating the flux above the 3σ detection limit ($F([\text{OIII}])_{\text{int}}$), the nuclear [OIII] fluxes ($F([\text{OIII}])_{\text{nuc}}$), integrated inside a circular aperture with radius of 100 parsecs centered at the nucleus, the [OIII] fluxes obtained from the literature ($F([\text{OIII}])_{\text{lit}}$), the integrated [OIII] luminosities (calculated assuming $H_0 = 75 \text{ km s}^{-1} \text{ Mpc}^{-1}$, which will be used throughout this paper) and the reference from which $F([\text{OIII}])_{\text{lit}}$ was obtained.

As a check on our flux calibration, we present in Figure 2 a comparison between the observed fluxes and the ones obtained from the literature. This Figure shows a good agreement between the two measurements, with most of the points lying close to the bisector line, or to the right of it. This indicates that on average our images get larger fluxes than the published ones - a result which is expected, since the ground based data were obtained from long-slit observations which would miss the most extended regions of emission. The average difference between the observed values and the published ones is 0.09 ± 0.25 dex for all the galaxies, 0.17 ± 0.26 dex for Seyfert 1's and 0.05 ± 0.23 dex for Seyfert 2's.

To address how representative the observed sample is in relation to the entire $60\mu\text{m}$ sample, and to investigate possible biases influencing our analysis, we compare the

properties of the 60 galaxies with observed [OIII] images to those of the galaxies in the 60 μ m sample which were not observed, as well as the properties of Seyfert 1's and Seyfert 2's with observed [OIII] images. We do not compare the observed sample to the entire 60 μ m sample, because all the values for that sample are repeated in this one, and such a comparison would be biased. Figure 3a (left) compares the distances of the galaxies in the 60 μ m sample and the observed sample, which show very similar distributions. The KS test shows, from the comparison between the observed sample and the galaxies which were not observed, that there is an 84.6% probability that two samples drawn from the same parent population would differ this much. This result shows that the observations were not biased towards galaxies closer or farther away from us. The comparison between the distances of Seyfert 1's and Seyfert 2's with observed [OIII] images (Figure 3b) gives a similar result, with the KS showing a 81.6% probability that two samples drawn from the same parent population would differ this much or more.

It is also important to verify if there are any selection biases in the luminosities of the observed galaxies, or in the limit of detection of extended emission in Seyfert 1's and Seyfert 2's. The comparison between the [OIII] luminosities of the observed sources and the entire 60 μ m sample, where we used [OIII] fluxes from the literature for the sources which were not observed by HST, is presented in Figure 4a. We can see in this Figure that there is a good agreement between the two samples. Comparing the luminosities of the observed galaxies with those of the galaxies which were not observed, the KS test gives 38.6% probability that two samples drawn from the same parent population would differ this much. In the case of Seyfert 1's and Seyfert 2's with observed [OIII] images, their distributions are shown in Figure 4b. We can see in this Figure that the two Seyfert types have similar distributions, with the KS test giving a 6.4% probability that two samples drawn from the same parent population would differ this much.

One of the major objectives of this survey is to compare the sizes of the NLR's of Seyfert 1's and Seyfert 2's. This requires us to show that there is no bias towards the detection of more extended emission in one type of Seyfert relative to the other. We do this by comparing the 3σ detection limit of the observed Seyfert 1's and Seyfert 2's. Since most of the images were obtained with the same instrument and with similar exposure times, most galaxies have very similar 3σ surface brightness detection limits, with a distribution peaked around 3.7×10^{-17} erg cm $^{-2}$ s $^{-1}$ pix $^{-1}$. The KS test shows that there is no statistically significant difference in the distribution of detection limit fluxes of Seyfert 1's and Seyfert 2's, with a probability of 35.4% that two sample drawn from the same parent population would differ as much as these two. However, since the distance of our galaxies vary by a factor of 10, a more important test consists of comparing the luminosities of the detection limits. We find that in our case they also are very similar, with the KS test showing a 96.4% probability that two samples drawn from the same parent population would differ this much or more.

The final [OIII] images of the galaxies are presented in Figures 5 through 14 (6 galaxies per Figure). The lowest

contour value of these images corresponds to the 3σ level above the background in surface brightness, and the following ones increase in powers of 2 times 3σ . We also indicate in these images the position of the nucleus, measured on the continuum images, the position angle of the host galaxy major axis, measured by Schmitt & Kinney (2000) on ground based images, and the position angle of the radio emission published in Kinney et al. (2000) and Schmitt et al. (2001). With the exception of MRK 348, we used radio jet position angles determined based on VLA measurements, because these observations correspond to dimensions similar to those sampled by the [OIII] images. In those cases where the jet changes direction (e.g. MCG+8-11-11, NGC 1068 and MRK 3), we plot the position angle value measured closer to the nucleus.

These [OIII] images were used to measure the extension of the emission in these galaxies. We measured the effective radius, extent of the photometric semi-major and semi-minor axes of the [OIII] emission, R_e , R_{Maj} and R_{Min} , respectively, as well as the position angle (PA) of the [OIII] major axis, and the offset between the galaxy nucleus and the center of the [OIII] emitting region. The effective radii were determined by integrating the [OIII] flux inside circular apertures, centered at the nucleus, with radii increasing in steps of 0.1 pixels. The aperture which contains half of the integrated [OIII] flux gives the value of R_e . The measurements of R_{Maj} , R_{Min} and the PA of the [OIII] emission were done directly by eye on the images, using as reference the 3σ contour levels. The measurement of the offset between the nucleus and the center of the [OIII] emission was done in the following way. Based on the [OIII] images, it is possible to divide the major axis of emission into two segments, one to each side of the nucleus. We call these segments X1 and X2, which correspond to the larger and smaller segment, respectively. The offset between the nucleus and the center of the [OIII] emitting region is calculated using the expression: Offset=(X1- R_{Maj})/ R_{Maj} , which gives the displacement in units of the semi-major axis of emission.

Table 3 gives the measured values of R_e , R_{Maj} , R_{Min} , PA, Offset from the nucleus to the [OIII] emission center, and the Figure number for the [OIII] image. Some of the galaxies in the sample have conically-shaped NLR's, however, their R_{Maj} is not always along the axis of the apparent cone. In these cases, Table 3 also gives the PA of the cone axis in parentheses in column 5.

5. INDIVIDUAL OBJECTS

In this section, we describe the observed emission of individual galaxies and give a brief review of some data in the literature. For each galaxy, we present the sizes of the major and minor [O III] emission axes, the PA of the major axis, discuss the structure of the NLR (e.g. apparent cone shape, or blobs of emission) and point out relations of these structures to the radio jet and host galaxy. It is not our intent to do a detailed study of the data available in the literature for each one of the galaxies. However, we make an effort to point out which galaxies have published radio images, as well as ground-based and HST narrow band images. Also, for the Seyfert 2's, we indicate which ones are known to show polarized broad emission lines.

The galaxies in this section are ordered by Right Ascen-

sion (Table 2). Notice that the dimensions given in this section correspond to the total extent of emission along the major and minor axis (based on the 3σ surface brightness contour), and not only the size of the semi major and minor axes (R_{Maj} and R_{Min}) given in Table 3.

5.1. MRK 348

This is a Seyfert 2 galaxy with polarized broad emission lines (Tran 1995). The HST [OIII] and $H\alpha + [NII]$ images were studied by Capetti et al. (1996) and Falcke, Wilson & Simpson (1998). The [OIII] emission (Figure 5 top left) is extended by $2.85''$ (840 pc) along P.A. = 185° , with a blob of emission at approximately $0.9''$ S of the nucleus. Along the perpendicular direction the emission is extended by $1.75''$ (510 pc). Close to the nucleus, the emission is extended along P.A. $\sim -10^\circ$, which is similar to the direction of the radio emission observed by Ulvestad et al. (1999). It is possible to draw a cone with opening angle 60° on top of the extended [OIII] emission.

5.2. MRK 573

This is a Seyfert 2 galaxy known from ground-based images to have extended [OIII] emission (Haniff et al. 1988; Pogge et al. 1993, 1995) aligned with the radio triple source observed by Ulvestad & Wilson (1984), and misaligned by 60° from the host galaxy major axis. The HST images of this galaxy were studied in detail by SK96, Capetti et al. (1996), Falcke et al. (1998) and Ferruit et al. (1999). Figure 5 (top right) shows that the emission is composed of several arches around the nucleus, with a total extent of $8.9''$ (2980 pc) along P.A. = 120° , and $3.7''$ (1250 pc) along the perpendicular direction. A cone with opening angle of 75° can be drawn on top of the [OIII] emission.

5.3. IRAS 01475-0740

This is a Seyfert 2 galaxy with strong radio emission (S01b; Thean et al. 2001), unresolved on VLA scales, and also known to have polarized broad emission lines (Tran 2001). The [OIII] emission (Figure 5; middle left) has a halo-like morphology with an average extent of $0.8''$ (275 pc).

5.4. ESO 153-G 20

The [OIII] image of this Seyfert 2 galaxy is presented in Figure 5 (middle right), where we can see that the bulk of the line emission comes from the inner $1''$ and is extended along P.A. = -100° , misaligned about 70° from the host galaxy major axis. Some diffuse emission is seen extending over a region of $\sim 1.85 \times 2.65''$ (710 \times 1010 pc) centered at the nucleus, with a major-axis at P.A. = -10° . A cone with opening angle of 80° can be drawn on top of the extended emission close to the nucleus.

5.5. MRK 590

This Seyfert 1 galaxy has a slightly extended NLR (Figure 5, bottom left), with dimensions of $1.1 \times 1.5''$ (560 \times 770 pc), and major axis along P.A. = -5° . This emission does not resemble a conically-shaped NLR. Most of the extended [OIII] emission comes from the region North of the nucleus and is misaligned by $\sim 50^\circ$ relative to the host galaxy major axis. The radio emission (S01b) is unresolved.

5.6. MRK 1040

The [OIII] image of this Seyfert 1 galaxy is presented in the bottom right panel of Figure 5. The [OIII] emission is extended and shaped like a cone with opening angle of 120° , apex at $\sim 0.6''$ NW of the nucleus, and the axis pointing towards the SE direction, perpendicular to the host galaxy disk. The emission along the apparent cone axis is extended by $1.1''$ (350 pc), and by $1.5''$ (480 pc) along the perpendicular direction. The radio emission of this galaxy is unresolved (S01b).

5.7. UGC 2024

This Seyfert 2 galaxy presents diffuse [OIII] emission with no clear conical shape. The emission is extended by $1.45 \times 2.6''$ (630 \times 1130 pc) with the major axis along P.A. = -35° , within 5° from the host galaxy major axis (Figure 6, top left). The emission along the host galaxy minor axis is extended by $1.45''$ (630 pc). This galaxy present only an unresolved nuclear radio source (S01b).

5.8. NGC 1068

The [OIII] image of this Seyfert 2 galaxy is shown in the top right panel of Figure 6. This image shows that most of the [OIII] emission originates in a V-shaped region with opening angle of 50° , extending for approximately $10''$ (750 pc) along P.A. = 35° , and $5.8''$ (430 pc) in the direction perpendicular to the cone. The direction of this emission is coincident with the radio jet observed by Wilson & Ulvestad (1982b). Emission extending to regions farther away from the nucleus can be seen towards the NE and SE. NGC 1068 is the most extensively studied Seyfert 2 galaxy in the literature. It was the first one where polarized broad emission lines were detected (Antonucci & Miller 1985), as well as the first one to be shown to have a conically shaped NLR (Pogge 1988a). The HST images of this galaxy were discussed in detail by Evans et al. (1991), Macchetto et al. (1994), Capetti, Axon & Macchetto (1997), Bruhweiler et al. (2001). Studies of the kinematics of the NLR gas show outflows and a strong interaction between the gas and the radio source (Axon et al. 1998, Cecil et al. 2002). The radio emission is extended along P.A. = 33° on the larger scales (Wilson & Ulvestad 1982b), but is aligned along the N-S direction in the nuclear region (Muxlow et al. 1996; Gallimore et al. 1996). The high resolution X-ray images obtained with Chandra (Young, Wilson & Shopbell 2001) also show extended emission aligned the radio and [OIII].

5.9. MRK 1058

This is a Seyfert 2 galaxy with faint and unresolved radio emission (S01b). The [OIII] image (Figure 6, middle left) shows that the line emission is extended by $1.4 \times 2.3''$ (470 \times 760 pc) along P.A. = 205° . This emission has a V-shaped morphology with opening angle of 55° , and is close to perpendicular to the host galaxy major axis. The peak of emission is concentrated around the nucleus with a second blob at $0.75''$ SW.

5.10. *MCG -02-08-039*

The middle left panel of Figure 6 presents the [OIII] image of this Seyfert 2 galaxy, which shows only diffuse emission around the nucleus, with a diameter of $\sim 2''$ (1160 pc). The radio emission is unresolved (S01b).

5.11. *UGC 2514*

This is a Seyfert 1 galaxy with slightly extended radio emission along $PA = 236^\circ$ (S01b). The [OIII] image (Figure 6, bottom left panel) shows that most of the line emission is displaced to the W of the nucleus, with two blobs separated by $\sim 0.6''$ along $PA = -70^\circ$. The emission is extended by $1.35''$ (350 pc) along this direction, and by $1.15''$ (290 pc) along $PA = 190^\circ$.

5.12. *IRAS 03106-0254*

Figure 6 (bottom right) shows the [OIII] image of this Seyfert 2 galaxy. The emission is extended by $0.9 \times 1.5''$ (470×790 pc) along $PA = 30^\circ$, which is at a direction similar to that of the extended radio emission (S01b), and misaligned by 45° from the host galaxy major axis.

5.13. *IRAS 03125+0119*

The [OIII] emission of this Seyfert 2 galaxy (Figure 7, top left) is diffuse, with the largest extension of $1.5''$ (700 pc) along the host galaxy major axis, and $1''$ (470 pc) along the minor axis. The radio emission is unresolved (S01b).

5.14. *MRK 607*

The top right panel of Figure 7 shows that the [OIII] emission of this Seyfert 2 galaxy is extended by $3.75''$ (660 pc) along the host galaxy major axis, and $1.35''$ (240 pc) along the minor axis. Most of the emission originates at the nucleus, or in a blob between $0.9-1''$ NW of the nucleus. The radio emission is unresolved (Nagar et al. 1999). Ferruit et al. (2000) present a detailed discussion of the HST images of this galaxy.

5.15. *ESO 116-G 18*

The [OIII] image of this Seyfert 2 galaxy (Figure 7, middle left) is extended by $1.7''$ (610 pc) along $PA = 75^\circ$, and $1''$ (360 pc) in the perpendicular direction. Most of the emission originates from regions N of the nucleus.

5.16. *NGC 1386*

This is a Seyfert 2 galaxy known, based on observations from the ground, to have extended [OIII] and radio emission (Weaver, Wilson & Baldwin 1991; Storchi-Bergmann et al. 1996). The image presented in Figure 7 (middle right panel) shows that the [OIII] emission consists of several blobs along the N-S direction, misaligned by 25° from the host galaxy major axis, and extending over a region of $5.9''$ (330 pc). The emission along the perpendicular direction is extended by only $1.6''$ (90 pc). There are 3 blobs of emission to the N of the nucleus, located at $0.8''$, $1.3''$ and $2.8''$, while to the S there is a blob at $1''$ and a ring of blobs at $2''$ from the nucleus. The direction of the extended [OIII] emission is similar to the extended radio emission detected by Nagar et al. (1999). Ferruit et al. (2000) present a detailed study of this and other HST narrow band images of this galaxy.

5.17. *ESO 33-G 02*

The [OIII] image of this Seyfert 2 galaxy is presented in the bottom left panel of Figure 7. The emission is distributed in a more or less homogeneous way around the nucleus, extended by $1 \times 1.45''$ (350×510 pc), with the major-axis along the N-S direction, perpendicular to the host galaxy major-axis. Some diffuse emission can be seen to the NE of the nucleus. The ground based [OIII] images published by Mulchaey et al. (1996a) show only slightly resolved emission.

5.18. *MCG -05-13-017*

This Seyfert 1 galaxy presents [OIII] emission homogeneously distributed around the nucleus (Figure 7 bottom right). This emission is elongated along the host galaxy major axis, extending for approximately $2''$ (500 pc) in this direction and by $1.5''$ (380 pc) along the minor axis. This galaxy has only unresolved nuclear radio emission (S01b).

5.19. *MCG +08-11-011*

Previous HST images obtained with WF/PC1 did not show any extended [OIII] emission (Bower et al. 1994; SK96) which was probably due to the strong spherical aberration of the pre-COSTAR images. Radio images from S01b show 3.6 cm emission extended for $3.5''$ along the N-S direction. Closer to the nucleus Ulvestad & Wilson (1986) showed that the radio structure consists of a triple source extended by $\sim 1''$ along $PA = 127^\circ$. The top left panel of Figure 8 presents the [OIII] image of this Seyfert 1 galaxy. We can see that most of the emission is extended close to the N-S direction, along $PA = 20^\circ$, aligned with the large-scale radio emission. The total extent of the emission in this direction is $3.6''$ (1450 pc), and $3''$ (1210 pc) along the perpendicular direction. South of the nucleus we see a CCD defect which could not be removed from the data, but also does not influence the results. A large portion of the emission is concentrated at the nucleus with a second blob of emission located at $0.7''$ N of it. Closer to the nucleus, we see two blobs of emission, one to each side of it, separated by $\sim 1''$ along $PA = 130^\circ$. These structures may be related to the nuclear triple radio source detected by Ulvestad & Wilson (1986).

5.20. *MRK 3*

The [OIII] image of this Seyfert 2 galaxy is S-shaped, with a clear conical NLR at regions close to the nucleus (Figure 8; top right). The major extent of the line emission is $2.2''$ (580 pc) along the E-W direction, while along the N-S direction it is extended by $1''$ (260 pc). The line emission is aligned with the radio emission described by Ulvestad & Wilson (1984). A detailed discussion of this galaxy is given by SK96 and Capetti et al. (1996). Capetti et al. (1999) and Ruiz et al. (2001) discuss the kinematics of the NLR gas, which is strongly influenced by the interaction with the radio emission.

5.21. *UGC 3478*

The middle left panel of Figure 8 shows that the [OIII] emission of this Seyfert 1 galaxy is diffuse, extended by $1.15 \times 1.65''$ (290×410 pc), with the major axis along $PA =$

55°. This emission is aligned close to the host galaxy major axis. The radio emission shows only an unresolved source (S01b).

5.22. *MRK 6*

Ground-based observations of this Seyfert 1 galaxy (Haniff et al. 1988) showed only an unresolved nuclear source. Our observations (Figure 8, middle right) show [OIII] emission extended by 3.2'' (1150 pc) along P.A.= -10°, a direction similar to that of the extended radio emission observed by S01b. The emission is concentrated at the nucleus, with a series of blobs around it and a finger of emission extending for 0.5'' towards P.A.= 210°. The largest blob is located 0.7'' N of the nucleus, and is probably related to the emission detected in the radio. Another small blob is observed at 0.5'' NW of the nucleus and is possibly related to the beginning of a transverse radio structure observed by Kukula et al. (1996) and S01b.

5.23. *Fairall 265*

The [OIII] image of this Seyfert 1 galaxy is presented in the bottom left panel of Figure 8. The emission is diffuse and extended by 2.9×3.45'' (1660×1970 pc) along PA= -20°.

5.24. *MRK 79*

This is a Seyfert 1 galaxy with extended radio emission along PA= 11° (Ulvestad & Wilson 1984; S01b; Thean et al. 2000), also known from ground-based images to have extended [OIII] emission (Haniff et al. 1988). Our [OIII] image (Figure 8 bottom right) is extended by 4.6'' (1980 pc) along the N-S direction, which appears closely related to the radio emission. To the S of the nucleus we see two blobs of emission, one at 0.6'' and another at 1.2'' from the nucleus. A larger number of structures is seen to the N, where we detect blobs at 0.5'', 0.9'' and 1.6''. The northern tip of the emission is separated by 2.5'' from the nucleus and is composed of several blobs along a 3.25'' region in the E-W direction.

5.25. *MRK 622*

Nagar et al. (1999) detected slightly resolved radio emission in this Seyfert 2 galaxy, extended along PA= 0°. Mulchaey et al. (1996a) found only halo like [OIII] emission in ground-based observations. Our [OIII] image (Figure 9 top left) is extended by 0.95×1.3'' (430×580 pc) along P.A.= 55°, perpendicular to the host galaxy major axis.

5.26. *ESO 18-G 09*

This Seyfert 2 galaxy has an apparent V-shaped [OIII] emission, with an opening angle of 45°, extended by 3'' (1040 pc) along PA= -30° (Figure 9 top right). One blob of emission is seen at 0.7'' NW of the nucleus and another one at the same distance towards the SE. Emission in the direction perpendicular to the apparent cone axis is extended by 1.1'' (380 pc).

5.27. *MCG -01-24-012*

The middle left panel of Figure 9 shows the [OIII] image of this Seyfert 2 galaxy. The emission is extended

for 1.15×2.3'' (440×880 pc) with the major axis along PA= 75°. Most of the emission is concentrated around the nucleus and in a blob at 0.5'' W of it. The radio emission is extended in the E-W direction (S01b).

5.28. *MRK 705*

Ground-based narrow band [OIII] images of this Narrow Line Seyfert 1 galaxy (Mulchaey et al. 1996a), as well as radio images (S01b), showed only an unresolved source. Our HST [OIII] image (Figure 9 middle right) is compact, extending for a diameter of 1.1'' (620 pc) around the nucleus.

5.29. *NGC 3281*

This Seyfert 2 galaxy was studied in detailed by Storchi-Bergmann, Wilson & Baldwin (1992), who used ground-based narrow band imaging and long-slit spectroscopy. These authors detected a cone of ionized gas extending up to 2 Kpc above the disk of the galaxy, and an outflow along the axis of this cone. The radio emission studied by S01b does not show any extended emission. Our [OIII] image (Figure 9 bottom left) confirms the ground-based [OIII] observations of Storchi-Bergmann et al. (1992), showing a conically-shaped NLR with opening angle ~ 80° towards the NE. The emission is extended by 3.9'' (800pc) along the cone axis, and 6.1'' (1260 pc) along the N-S direction. The emission inside the cone can be divided into two major structures, one consisting of several blobs close to the nucleus, and the other one being a ridge of emission 2'' NE of the nucleus, parallel to the host galaxy major axis. We also detect a small blob of emission at 4.5'' S of the nucleus, corresponding to the counter ionization cone, which is mostly hidden by the host galaxy disk. The emission observed by HST seems to be less extended than that observed by Storchi-Bergmann et al. (1992), however, this can be due to the field of view of the Liner Ramp Filter.

5.30. *NGC 3393*

The [OIII] emission of this Seyfert 2 galaxy (Figure 9 bottom right) is S-shaped, extended by 5.3'' (1410 pc) along PA= 65° and 2.8'' (740 pc) along the perpendicular direction. The S structure surrounds the radio emission observed by S01b. A detailed discussion of the NLR of this galaxy, involving the observations presented here, ground based imaging and spectroscopy, and radio continuum observations, is presented by Cooke et al. (2000). This galaxy is known to have polarized broad emission lines (Kay, Tran & Magalhães 2002).

5.31. *UGC 6100*

Figure 10, top left panel, presents the [OIII] image of this Seyfert 2 galaxy. The emission is S-shaped and extended by 1.3×3.5'' (740×1990 pc) along the N-S direction. The radio image presented by Kukula et al. (1995) is slightly resolved.

5.32. *NGC 3516*

The [OIII] image of this Seyfert 1 galaxy is presented in the top right panel of Figure 10. The emission is S-shaped, extended by 13.6'' (2330 pc) along PA= 20°. The extension of the emission along the E-W direction at the

bottom and top of the S-shaped structure is $6.9''$ (1180 pc). A detailed study of the NLR of this source is presented by Ferruit et al. (1998). Nagar et al. (1999) detected extended radio emission along $PA = 10^\circ$.

5.33. NGC 3783

This Seyfert 1 galaxy has a halo like NLR with [OIII] emission extended over a region of $1.9''$ (310 pc) in diameter around the nucleus (Figure 10 middle left). Ground based narrow band observations by Winge et al. (1992) found only an unresolved source, and the radio emission also is unresolved (S01a).

5.34. MRK 766

The [OIII] emission of this Seyfert 1 galaxy is concentrated around the nucleus, as can be seen in the middle right panel of Figure 10. It has a halo-like morphology, with a diameter of $1.9''$ (470 pc). The radio emission is slightly extended along $P.A. = 32^\circ$ (Nagar et al. 1999).

5.35. NGC 4388

This Seyfert 2 was one of the first galaxies where a conically shaped NLR was detected (Pogge et al. 1988b; Yoshida et al. 2002). Galactic scale outflows have been detected by Veilleux et al. (1999), and Matt et al. (1994) detected soft X-ray emission extended over 4.5 kpc in observations with ROSAT. The observations presented here, as well as radio observations, are discussed in detail by Falcke et al. (1998). This galaxy is also known to have polarized broad emission lines (Young et al. 1996). The [OIII] image (Figure 10 bottom left) shows a V-shaped NLR with opening angle of 90° towards the S, extended over $6.1''$ (1000 pc) in this direction. The extent along the perpendicular direction is $7.8''$ (1270 pc). Most of the emission comes from regions S of the nucleus, except for some emission corresponding to the counter cone, which is observed to the NE side of the nucleus. Most of the counter cone emission is obscured by the host galaxy.

5.36. NGC 4507

The [OIII] image of this Seyfert 2 galaxy is presented in the bottom right panel of Figure 10. We can see that the emission is elongated along $PA = -35^\circ$ in the inner $\sim 2''$ region, becoming more circular in the outer regions. The major extent of the emission is $3.5''$ (800 pc). The bulk of the emission is related to the nucleus and a blob located at $1''$ to the NW. This galaxy show broad emission lines in polarized light (Moran et al. 2000).

5.37. NGC 4593

The [OIII] image of this Seyfert 1 galaxy (Figure 11 top left) has a halo-like morphology, slightly elongated along $PA = 100^\circ$, which is a direction similar to the host galaxy major axis. The extent of the emission in this direction is $1.7''$ (300 pc), while along the minor axis the emission is extended by $1.35''$ (240 pc). The radio emission of this galaxy is unresolved (S01b).

5.38. NGC 4968

Figure 11, top right panel presents the [OIII] image of this Seyfert 2 galaxy. The major axis of the [OIII] emitting region is extended by $2.2''$ (420 pc) along $PA = 40^\circ$ and $1.3''$ (250 pc), along the perpendicular direction. Previous ground-based observation did not detect any extended [OIII] emission (Pogge 1989), and found only some marginally extended radio emission (S01b). A more detailed description of the NLR of this galaxy is given by Ferruit et al. (2000).

5.39. IRAS 13059-2407

The [OIII] emission of this Seyfert 2 galaxy is faint, mostly displaced to the W relative to the peak of continuum emission, and extended by $0.5 \times 1.35''$ (140×360 pc) along $PA = -10^\circ$ (Figure 11 middle left). The emission in this direction is divided into two blobs, separated by $0.35''$. The radio emission of this galaxy is unresolved (S01b).

5.40. MCG -6-30-15

The middle right panel of Figure 11 presents the [OIII] image of this Seyfert 1 galaxy. The emission is extended by $1.5 \times 3.9''$ (230×590 pc), with the major axis of the [OIII] emission at $P.A. = -65^\circ$. This direction is at 10° from the host galaxy major axis. The radio emission of this galaxy is unresolved (Nagar et al. 1999), and a detailed description of the NLR emission is given by Ferruit et al. (2000).

5.41. NGC 5347

Ground-based narrow-band images of this Seyfert 2 galaxy (Pogge 1989; González Delgado & Pérez 1996) show a double structure along $PA = 25^\circ$. This galaxy is also known to have polarized broad emission lines (Moran et al. 2001). The nuclear radio emission is unresolved (S01b). Our [OIII] image (Figure 11 bottom left) confirms the two structures detected on ground based images, a nuclear V-shaped structure with opening angle $\sim 60^\circ$, extending by $1.75''$ (260 pc) along $PA = 30^\circ$, and the second structure at $2.4''$ (370 pc) NE from the nucleus, which has a width of $0.35''$ (50 pc) along the radial direction from the nucleus and a length of $2.45''$ (370 pc).

5.42. IRAS 14082+1347

All the [OIII] in this Seyfert 2 galaxy (Figure 11 bottom right) originates in a region $\sim 1''$ S of the nucleus ($PA = 165^\circ$). It has a major extent of $1''$ (310 pc) in the N-S direction and $0.75''$ (230 pc) in the E-W direction. The radio emission of this galaxy is unresolved (S01b).

5.43. NGC 5548

The [OIII] emission from this Seyfert 1 galaxy has a halo-like morphology (Figure 12 top left), with a diameter of $1.3''$ (450 pc) around the nucleus. It also presents some low surface brightness fingers of emission extending by $2.7''$ (900 pc) in the N-S direction. The radio emission extends for $18''$ along $PA = -15^\circ$ (Wilson & Ulvestad 1982a). Ground-based observations (Wilson et al. 1989) detected low intensity [OIII] emission which is not detected by the current observations. This could be due to differences in the sensitivity of the two observations.

5.44. *IRAS 14317-3237*

Figure 12, top right panel presents the [OIII] image of this Seyfert 2 galaxy, which is elongated by $1.4''$ (690 pc) along $PA = -5^\circ$, a direction similar to the observed extended radio emission (S01b). The emission along the perpendicular direction, close to the host galaxy minor axis, is extended by $0.75''$ (370 pc).

5.45. *UGC 9826*

The [OIII] emission of this Seyfert 1 galaxy (Figure 12 middle left) has a halo morphology with a slightly larger extent of $1.55''$ (870 pc) along the host galaxy major axis, and $0.9''$ (510 pc) along the minor axis. The radio emission is unresolved (S01b).

5.46. *UGC 9944*

This Seyfert 2 galaxy has a conically shaped NLR aligned along $PA = 90^\circ$, with an opening angle of 110° (Figure 12 middle right). The extent of the NLR in this direction is $1.5''$ (710 pc), while in the perpendicular direction it is extended by $2''$ (950 pc). The radio emission of this galaxy consists of a triple source extended by approximately $8''$ along $PA = 67^\circ$. We do not detect any [OIII] emission related to the outermost radio emission.

5.47. *IRAS 16288+3929*

The bottom left panel of Figure 12 presents the [OIII] image of this Seyfert 2 galaxy. The emission is extended by $1.6 \times 2.7''$ (940×1590 pc) along $PA = 65^\circ$. The radio emission is unresolved (S01b).

5.48. *IRAS 16382-0613*

The [OIII] emission of this Seyfert 2 galaxy (Figure 12 bottom right) is elongated along $PA = 15^\circ$, extended by $1.2''$ (650 pc) in this direction and $0.9''$ (480 pc) in the perpendicular direction. The radio emission, observed by S01b, is unresolved.

5.49. *UGC 10889*

The top left panel of Figure 13 presents the [OIII] image of this Seyfert 2 galaxy. The largest extent of the emission is $1.25''$ (680 pc) along $PA = 95^\circ$ and consists of two blobs, one centered at the nucleus and one $0.4''$ W of it. The radio emission is unresolved (S01b).

5.50. *MCG +03-45-003*

The [OIII] emission of this Seyfert 2 galaxy (Figure 13 top right) is extended by $3''$ (1410 pc) along $PA = 15^\circ$, and $1.3''$ (600 pc) in the perpendicular direction. The emission is distributed among several blobs, one centered at the nucleus, one $0.75''$ S, one $0.35''$ N and another one $1''$ N. The radio emission of this galaxy was studied by S01b, which found only an unresolved nuclear source.

5.51. *Fairall 51*

Figure 13, middle left panel shows the [OIII] image of this Seyfert 1 galaxy. The emission is extended by $2.65''$ (730 pc) along the host galaxy major axis. Most of the emission is concentrated at the $1''$ region around the nucleus, with a finger like structure extending to the S. The overall emission can be fit by an apparent cone with opening angle of 110° and the axis along the SW direction.

5.52. *NGC 6860*

Ground-based narrow-band images of this Seyfert 1 galaxy, published by L  pari, Tsvetanov & Macchetto (1993), show emission extended by $10''$ along the E-W direction. Our [OIII] image (Figure 13 middle right) shows emission along the same direction, consisting of an S-shaped NLR along $PA = 85^\circ$, extended by $\sim 4.5''$ in this direction (1300 pc), and $2.4''$ (690 pc) in the perpendicular direction. Most of the emission is concentrated at the nucleus and in a blob $0.4''$ E, with a second more extended and fainter structure at $0.9''$ E. To the W of the nucleus we see a long arm of emission extending by $\sim 0.8''$ and a more diffuse structure at $2.5''$.

5.53. *UGC 11630*

Most of the [OIII] emission of this Seyfert 2 galaxy (Figure 13 bottom left) is displaced to the E of the nucleus. It has a major extent of $1.6''$ (380 pc) along $PA = 30^\circ$ and is divided into two blobs separated by $0.6''$. The radio emission of this galaxy is unresolved (S01b).

5.54. *IC 5063 = PKS 2048-57*

The ground-based [OIII] image of this Seyfert 2 galaxy shows emission extended over a region larger than $\sim 30''$, along $P.A. = -65^\circ$ (Morganti et al. 1998; Morganti et al. 1999). The line emission is aligned with the radio emission and the host galaxy major-axis. This galaxy is also known to have polarized broad emission lines (Inglis et al. 1993). Our [OIII] image confirms the ground based results, but shows only a much smaller portion of the extended emission, due to the field of view of the Linear Ramp Filter (Figure 13 bottom right). This emission can be represented by a bicone centered at the nucleus, with opening angle of 60° , extending by $12''$ (2640 pc) along $PA = -65^\circ$ and $\sim 3''$ (660 pc) along the perpendicular direction. At distances larger than $3''$ N of the nucleus the emission seems to split on the two sides of the host galaxy major axis, giving it the appearance of an X-shaped NLR.

5.55. *NGC 7212*

This is a Seyfert 2 galaxy in an interacting system (Schmitt & Kinney 2000), which presents polarized broad emission lines (Tran 1995). The [OIII] emission of this Seyfert 2 galaxy (Figure 14 top left) is extended along $PA = 170^\circ$, with dimensions of $2.1''$ by $4.8''$ (1080×2480 pc). The emission is composed of several individual blobs to the N and S of the nucleus. This emission is aligned with the radio emission. A detailed study of the narrow band and radio images of this galaxy is presented by (Falcke et al. 1998).

5.56. *NGC 7213*

The [OIII] emission of this Seyfert 1 galaxy (Figure 14 top right) has a halo like morphology, homogeneously distributed around the nucleus, with a diameter of $1.1''$ (130 pc). The radio emission is unresolved (S01b, Thean et al. 2000). The kinematics and the chemical abundance of the gas in this galaxy was studied by Storchi-Bergmann et al. (1996).

5.57. *MRK 915*

Figure 14, middle left panel, presents the [OIII] image of this Seyfert 1 galaxy. The emission is very irregular, with a major extent of $4.1''$ (1910 pc) along $PA = 5^\circ$, and $2.6''$ (1220 pc) in the perpendicular direction. Most of the emission comes from the nucleus and a structure $0.65''$ to the SW. This structure has $1.3''$ in length ($PA = 140^\circ$) and $0.4''$ in width. Another blob of emission is seen at $1.1''$ to the N of the nucleus. The radio emission, observed by S01b, shows an unresolved nuclear structure and a faint tail of emission extending to the SW.

5.58. *UGC 12138*

The [OIII] emission of this Seyfert 1 galaxy (Figure 14 middle right) has a diffuse morphology with a diameter of $1.5''$ (710 pc) centered at the nucleus. The radio emission observed by Kukula et al. (1995) is unresolved.

5.59. *UGC 12348*

Figure 14, bottom left panel, presents the [OIII] image of this Seyfert 2 galaxy, which is elongated along $PA = 100^\circ$ with an extent of $1.15'' \times 2.2''$ (560×1080 pc). The radio emission, observed by S01b, is unresolved.

5.60. *NGC 7674*

This Seyfert 2 galaxy was observed to have polarized broad emission lines by Miller & Goodrich (1990). The radio emission was studied by Unger et al. (1988), Neff & Hutchings (1992) and Kukula et al. (1995), who found a double source separated by $\sim 0.5''$ along $PA = 117^\circ$ and a smaller component to the E of the nucleus. Ground-based spectroscopy shows young stars around the nucleus of this galaxy (González Delgado, Heckman & Leitherer 2001). The HST [OIII] image, presented in the bottom right panel of Figure 14, is extended by $4.4''$ (2480 pc) along $PA = 120^\circ$, which is a direction similar to that of the extended radio emission, and $2.7''$ (1520 pc) along the

perpendicular direction. One can also see in this image, at $1.3''$ to the NW of the nucleus, along the host galaxy major axis, a small loop and a hole in the emission.

6. SUMMARY

We have presented the results of an imaging survey of extended [OIII] emission in a sample of 60 Seyfert galaxies (22 Seyfert 1's and 38 Seyfert 2's). We discussed the details of the different observations used in this paper, the reduction and calibration techniques used to create the continuum-subtracted [OIII] images, and the measurements done with these images. By comparing the redshifts and [OIII] luminosities of the observed galaxies to those of the entire $60\mu\text{m}$ sample (Kinney et al. 2000), we find a good agreement, indicating that the observed galaxies are a representative subsample and can be used to draw statistical results. Furthermore, a comparison between the distances, [OIII] luminosities and detection limits of the Seyfert 1's and Seyfert 2's with observed [OIII] images shows a good agreement between these two groups of galaxies, which suggests that selection effects will not influence the results of studies which use these data to compare their properties. This paper also gives a description of the structure of the NLR of these galaxies, together with a brief review of the relevant data available in the literature.

We would like to thank J. S. Ulvestad and J. E. Pringle for comments. This work was partially supported by the NASA grants HST-GO-8598.07-A and AR-8383.01-97A. The National Radio Astronomy Observatory is a facility of the National Science Foundation, operated under cooperative agreement by Associated Universities, Inc. This research made use of the NASA/IPAC Extragalactic Database (NED), which is operated by the Jet Propulsion Laboratory, Caltech, under contract with NASA. J.D.'s work was supported by the National Science Foundation, through its Research Experience for Undergraduates program.

REFERENCES

- Antonucci, R. R. J. 1993, *ARA&A*, 31, 473
 Antonucci, R. R. J. & Miller, J. S. 1985, *ApJ*, 297, 621
 Axon, D. J., Marconi, A., Capetti, A., Macchetto, F., Schreier, E. & Robinson, A. 1998, *ApJ*, 496, L75
 Bower, G. A., Wilson, A. S., Mulchaey, J. S., Miley, G. K., Heckman, T. M. & Krolik, J. H. 1994, *AJ*, 107, 1686
 Bruhweiler, F. C., Miskey, C. L., Smith, A. M., Landsman, W. & Malumuth, E. 2001, *ApJ*, 546, 866
 Capetti, A., Axon, D. J. & Macchetto, F. 1997, *ApJ*, 487, 560
 Capetti, A., Axon, D. J., Macchetto, F., Marconi, A. & Winge, C. 1999, *ApJ*, 519, 134
 Capetti, A., Axon, D. J., Macchetto, F., Sparks, W. B., & Boksenberg, A. 1996, *ApJ*, 466, 169
 Cecil, G., Dopita, M. A., Groves, B., Wilson, A. S., Ferruit, P., Pécontal, E. & Binette, L. 2002, *ApJ*, 568, 627
 Cooke, A. J., Baldwin, J. A., Ferland, G. J., Netzer, H. & Wilson, A. S. 2000, *ApJS*, 129, 517
 Cruz-Gonzalez, I., Carrasco, L., Serrano, A., Guichard, J., Dultzin-Hacyan, D. & Bisiacchi, G. F. 1994, *ApJS*, 94, 47
 de Grijs, M. H. K., Keel, W. C., Miley, G. K., Goudfrooij, P., & Lub, J. 1992, *A&AS*, 96, 389
 de Grijs, M. H. K., Miley, G. K., & Lub, J. 1987, *A&AS*, 70, 95
 Evans, I. N., Ford, H. C., Kinney, A. L., Antonucci, R. R. J., Armus, L. & Caganoff, S. 1991, *ApJ*, 369, L27
 Falcke, H., Wilson, A. S. & Simpson, C. 1998, *ApJ*, 502, 199
 Ferruit, P., Wilson, A. S., & Mulchaey, J. 1998, *ApJ*, 509, 646
 Ferruit, P., Wilson, A. S., & Mulchaey, J. 2000, *ApJS*, 128, 139
 Ferruit, P., Wilson, A. S., & Falcke, H., Simpson, C., Pécontal, E. & Durret, F. 1999, *MNRAS*, 309, 1
 Gallimore, J. F., Baum, S. A., O'Dea, C. P. & Pedlar, A. 1996, *ApJ*, 458, 136
 González Delgado, R. M., Heckman, T. M. & Leitherer, C. 2001, *ApJ*, 546, 845
 González Delgado, R. M. & Pérez, E. 1996, *MNRAS*, 280, 53
 Haniff, C. A., Wilson, A. S., & Ward, M. J. 1988, *ApJ*, 334, 104
 Ho, L. C. & Ulvestad, J. S. 2001, *ApJS*, 133, 77
 Inglis, M., Hough, J. H., Axon, D. J., Bailey, J., & Ward, M. J. 1993, *MNRAS*, 263, 895
 Kay, L. E., Tran, H. D. & Magalhães 2002, *AAS*, 200, 0501
 Kinney, A. L., Schmitt, H. R., Clarke, C. J., Pringle, J. E., Ulvestad, J. S. & Antonucci, R. R. J. 2000, *ApJ*, 537, 152
 Kukula, M. J., Holloway, A. J., Pedlar, A., Meaburn, J., Lopez, J. A., Axon, D. J., Schilizzi, R. T. & Baum, S. A. 1996, *MNRAS*, 280, 1283
 Kukula, M. J., Pedlar, A., Baum, S. A. & O'Dea, C. P. 1995, *MNRAS*, 276, 1262
 Lipari, S. Tsvetanov, Z. & Macchetto, F. 1993, *ApJ*, 405, 186
 Macchetto, F., Capetti, A., Sparks, W. B., Axon, D. J. & Boksenberg, A. 1994, *ApJ*, 435, L15
 Matt, G., Piro, L., Antonelli, L. A., Fink, H. H., Meurs, E. J. A. & Perola, G. C. 1994, *A&S*, 292, L13
 Miller, J. S. & Goodrich, R. W. 1990, *ApJ*, 355, 456
 Moran, E. C., Barth, A. J., Kay, L. E. & Filippenko, A. V. 2000, *ApJ*, 540, L73

- Moran, E. C., Kay, L. E., Davis, M., Filippenko, A. V. & Barth, A. J. 2001, *ApJ*, 556, L75
- Morganti, R., Tsvetanov, Z. I., Gallimore, J. & Allen, M. G. 1999, *A&AS*, 137, 457
- Morganti, R., Oosterloo, T. & Tsvetanov, Z. I. 1998, *AJ*, 115, 915
- Mulchaey, J. S., Wilson, A. S., & Tsvetanov, Z. I. 1996a, *ApJS*, 102, 309
- Mulchaey, J. S., Wilson, A. S., & Tsvetanov, Z. I. 1996b, *ApJ*, 467, 197
- Muxlow, T. W. B., Pedlar, A., Holloway, A. J., Gallimore, J. F. & Antonucci, R. R. J. 1996, *MNRAS*, 278, 854
- Nagar, N. M., Wilson, A. S., Mulchaey, J. S. & Gallimore, J. F. 1999, *ApJS*, 120, 209
- Neff, S. G. & Hutchings, J. B. 1992, *AJ*, 103, 1746
- Neugebauer, G. et al. 1980, *ApJ*, 238, 502
- Pogge, R. W. 1988a, *ApJ*, 328, 519
- Pogge, R. W. 1988b, *ApJ*, 332, 702
- Pogge, R. W. 1989, *ApJ*, 345, 730
- Pogge, R. W. & De Robertis M. M. 1993, *ApJ*, 404, 563
- Pogge, R. W. & De Robertis M. M. 1995, *ApJ*, 451, 585
- Ruiz, J. R., Crenshaw, D. M., Kraemer, S. B., Bower, G. A., Gull, T. R., Hutchings, J. B., Kaiser, M. E. & Weistrop, D. 2001, *AJ*, 122, 2961
- Schmitt, H. R., Antonucci, R. R. J., Ulvestad, J. S., Kinney, A. L., Clarke, C. J. & Pringle, J. E. 2001a, *ApJ*, 555, 663
- Schmitt, H. R. & Kinney, A. L. 1996, *ApJ*, 463, 498
- Schmitt, H. R. & Kinney, A. L. 2000, *ApJS*, 128, 479
- Schmitt, H. R., Ulvestad, J. S., Antonucci, R. R. J. & Kinney, A. L. 2001b, *ApJS*, 132, 199
- Storchi-Bergmann, T., Rodríguez-Ardila, A., Schmitt, H. R., Wilson, A. S. & Baldwin, J. A. 1996, *ApJ*, 472, 83
- Storchi-Bergmann, T., Wilson, A. S. & Baldwin, J. A. 1992, *ApJ*, 396, 45
- Thean, A., Pedlar, A., Kukula, M. J., Baum, S. A. & O'Dea, C. P. 2000, *MNRAS*, 314, 573
- Tran, H. D. 1995, *ApJ*, 440, 578
- Tran, H. D. 2001, *ApJ*, 554, L19
- Ulvestad, J. S. & Wilson, A. S. 1984, *ApJ*, 278, 544
- Ulvestad, J. S. & Wilson, A. S. 1986, *MNRAS*, 218, 711
- Ulvestad, J. S., Wrobel, J. M., Roy, A. L., Wilson, A. S., Falcke, H. & Krichbaum, T. P. 1999, *ApJ*, 517, L81
- Unger, S. W. 1988, *MNRAS*, 234, 745
- Urry, C. M., & Padovani, P. 1995, *PASP*, 107, 803
- Veilleux, S., Bland-Howthorn, J., Cecil, G., Tully, R. B. & Miller, S. T. 1999, *ApJ*, 520, 111
- Weaver, K. A., Wilson, A. S. & Baldwin, J. A. 1991, *ApJ*, 366, 50
- Whittle, M. 1992, *ApJS*, 79, 49
- Wilson, A. S. & Ulvestad, J. S. 1982a, *ApJ*, 260, 56
- Wilson, A. S. & Ulvestad, J. S. 1982b, *ApJ*, 263, 576
- Wilson, A. S., Ward, M. J., & Haniff, C. A. 1988, *ApJ*, 334, 121
- Wilson, A. S., Wu, X., Heckman, T. M., Baldwin, J. A. & Balick, B. 1989, *ApJ*, 339, 729
- Winge, C., Pastoriza, M. G., Storchi-Bergmann, T. & Lipari, S. 1992, *ApJ*, 393, 98
- Young, S., Hough, J. H., Efsthathiou, A., Wills, B. J., Bailey, J. A., Ward, M. J., & Axon, D. J. 1996, *MNRAS*, 281, 1206
- Young, A. J., Wilson, A. S. & Shopbell, P. L. 2001, *ApJ*, 556, 6
- Yoshida, M. et al. 2002, *ApJ*, 567, 118

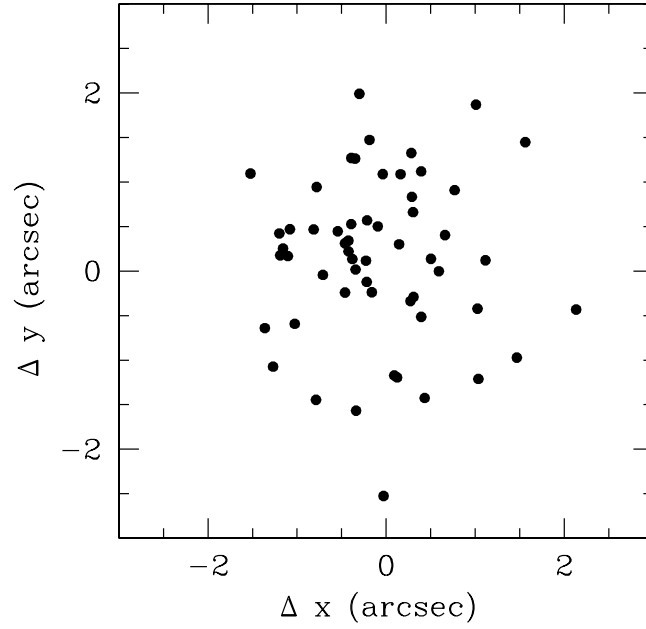


FIG. 1.— Difference between the expected and observed position of the source in the detector. This plot excludes the deviant point of NGC 4968 at $\Delta X = -5.41''$ and $\Delta Y = -3.84''$.

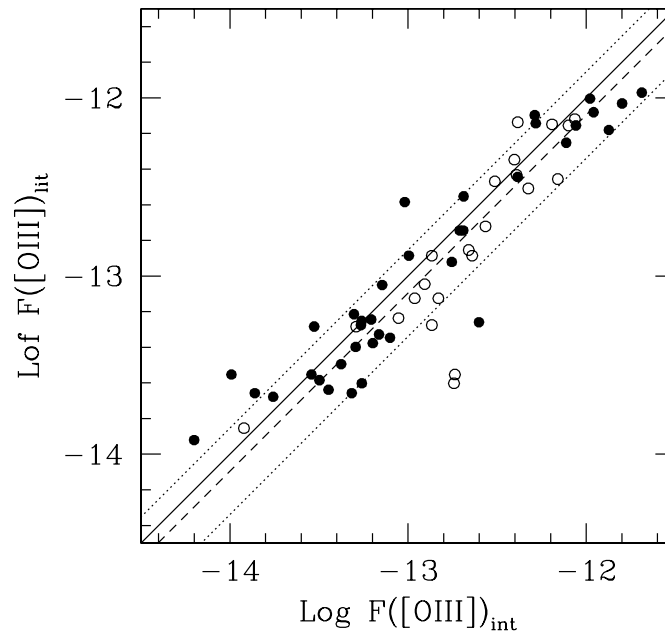


FIG. 2.— Comparison between the logarithm of the observed integrated [OIII] fluxes ($F([OIII])_{int}$) and the logarithm of the [OIII] fluxes obtained from the literature ($F([OIII])_{lit}$). Open symbols represent Seyfert 1's and filled ones Seyfert 2's. The solid line is the bisector line. The dashed line represents the average difference between the observed and published [OIII] fluxes, and the dotted lines represent the 1σ deviation.

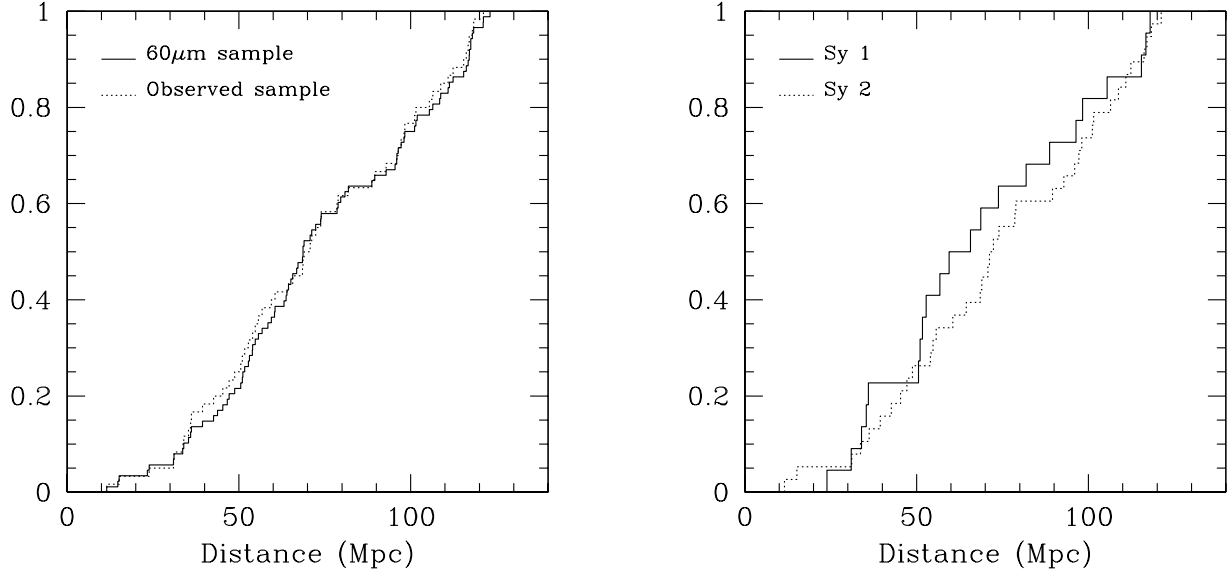


FIG. 3.— Left: The cumulative distribution of distances for the galaxies with [OIII] images (dotted line), and the $60\mu\text{m}$ sample (solid line). Right: The cumulative distribution of distances for the Seyfert 2 (dotted line) and Seyfert 1 galaxies (solid line) with [OIII] images.

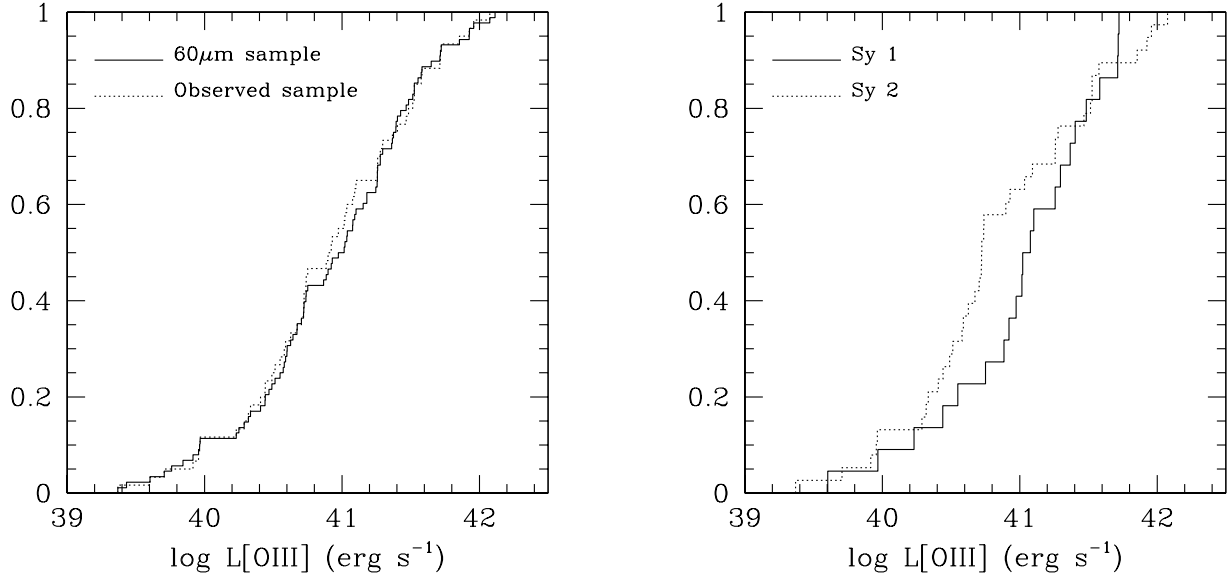


FIG. 4.— Same as Figure 3, but for the logarithm of the integrated [OIII] luminosities.

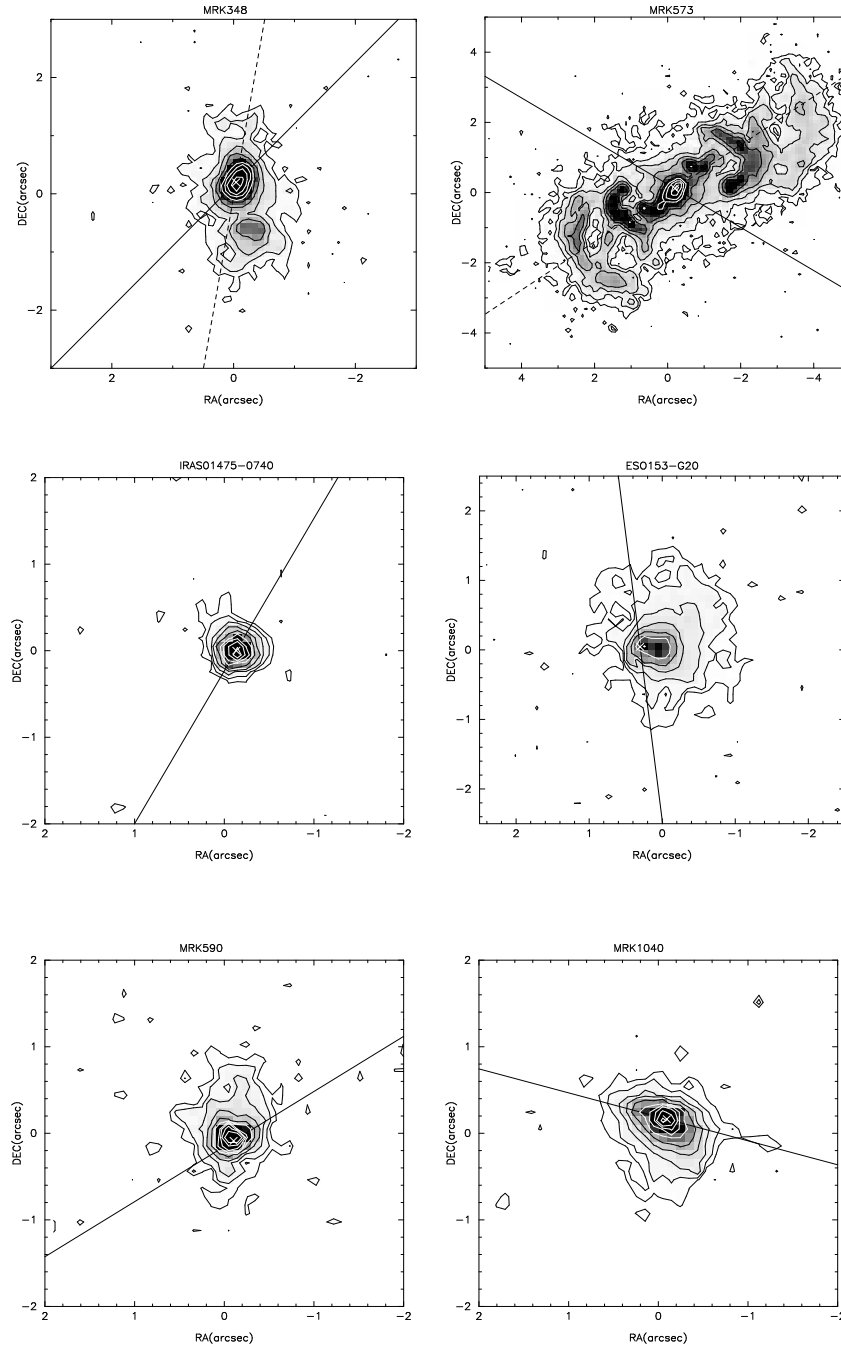


FIG. 5.— [OIII] continuum-subtracted image of MRK 348, MRK 573, IRAS 01475-0740, ESO 153-G 20, MRK 590, MRK 1040. The contours start at the 3σ level above the background and increase in powers of 2 times 3σ ($3\sigma \times 2^n$). The position of the nucleus, measured in the continuum images, is plotted as a white cross. The position-angle of the host galaxy major axis is shown as a solid line crossing the figure through the nucleus. For those galaxies with extended radio emission, we present the direction of the jet as a dashed line. North is up and East to the left.

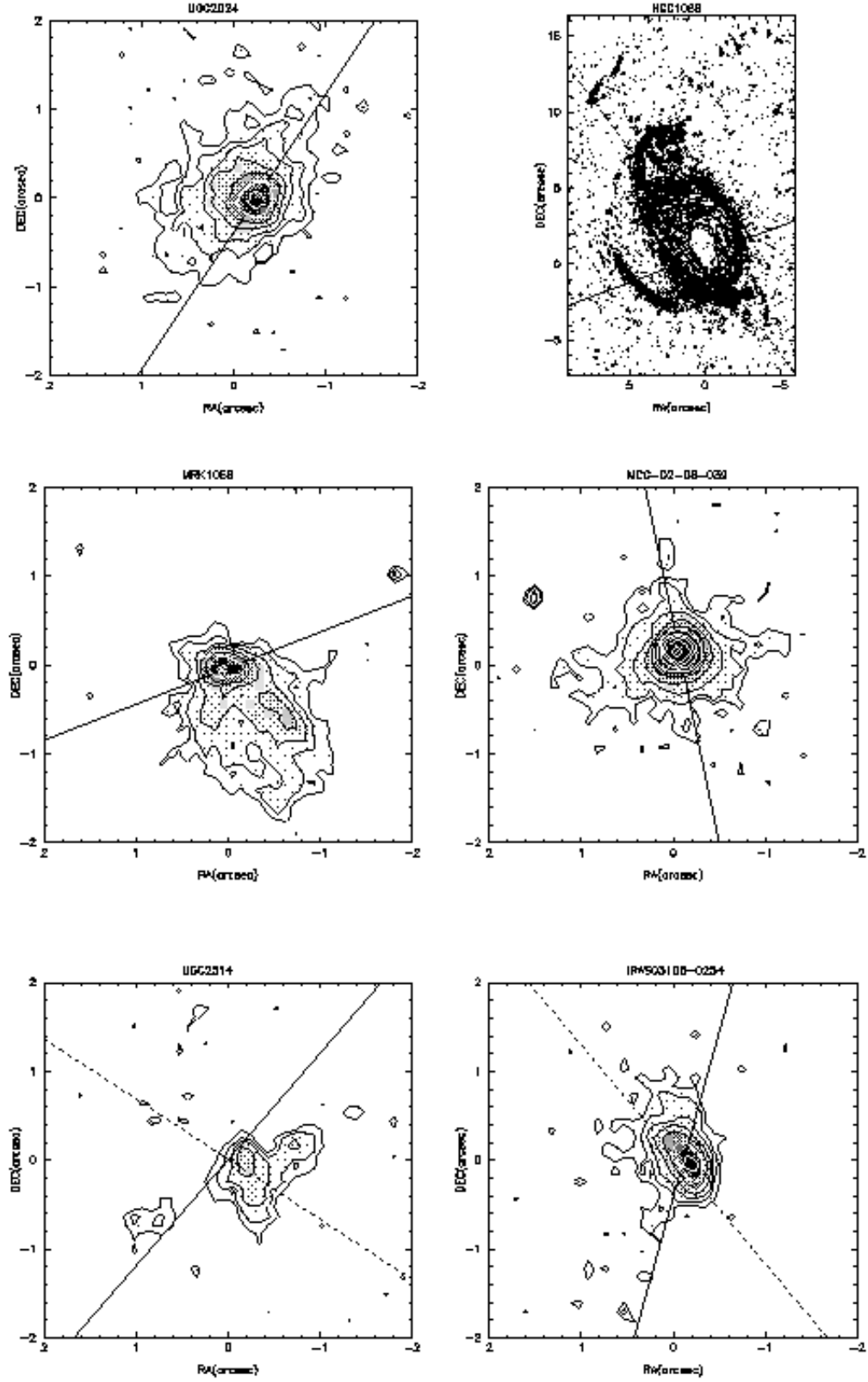


FIG. 6.— Same as Figure 5 for UGC 2024, NGC 1068, MRK1058, MCG-02-08-039, UGC 2514 and IRAS 03106-0254.

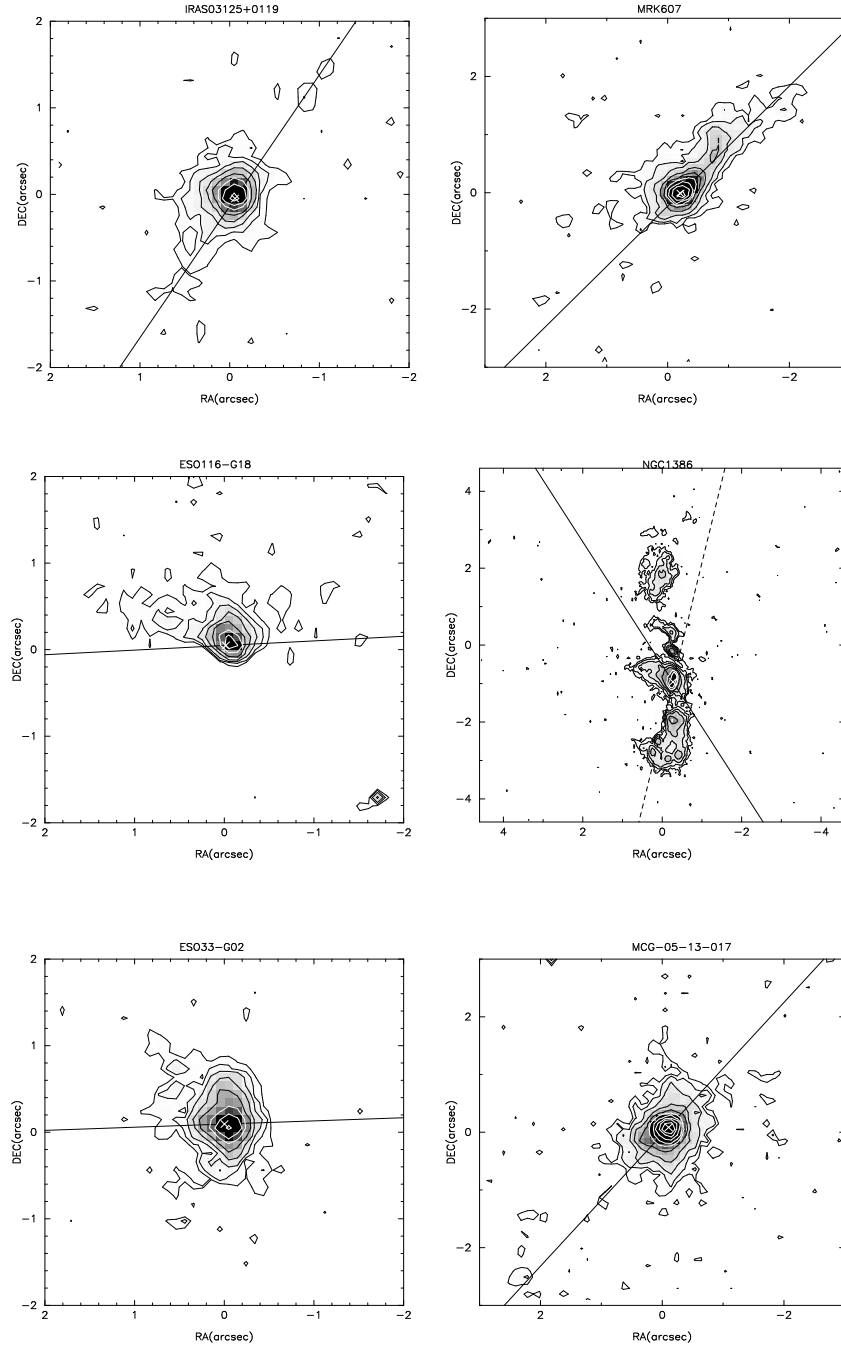


FIG. 7.— Same as Figure 5 for IRAS 03125+0119, MRK 607, ESO 116-G 18, NGC 1386, ESO 33-G 02 and MCG -05-13-017.

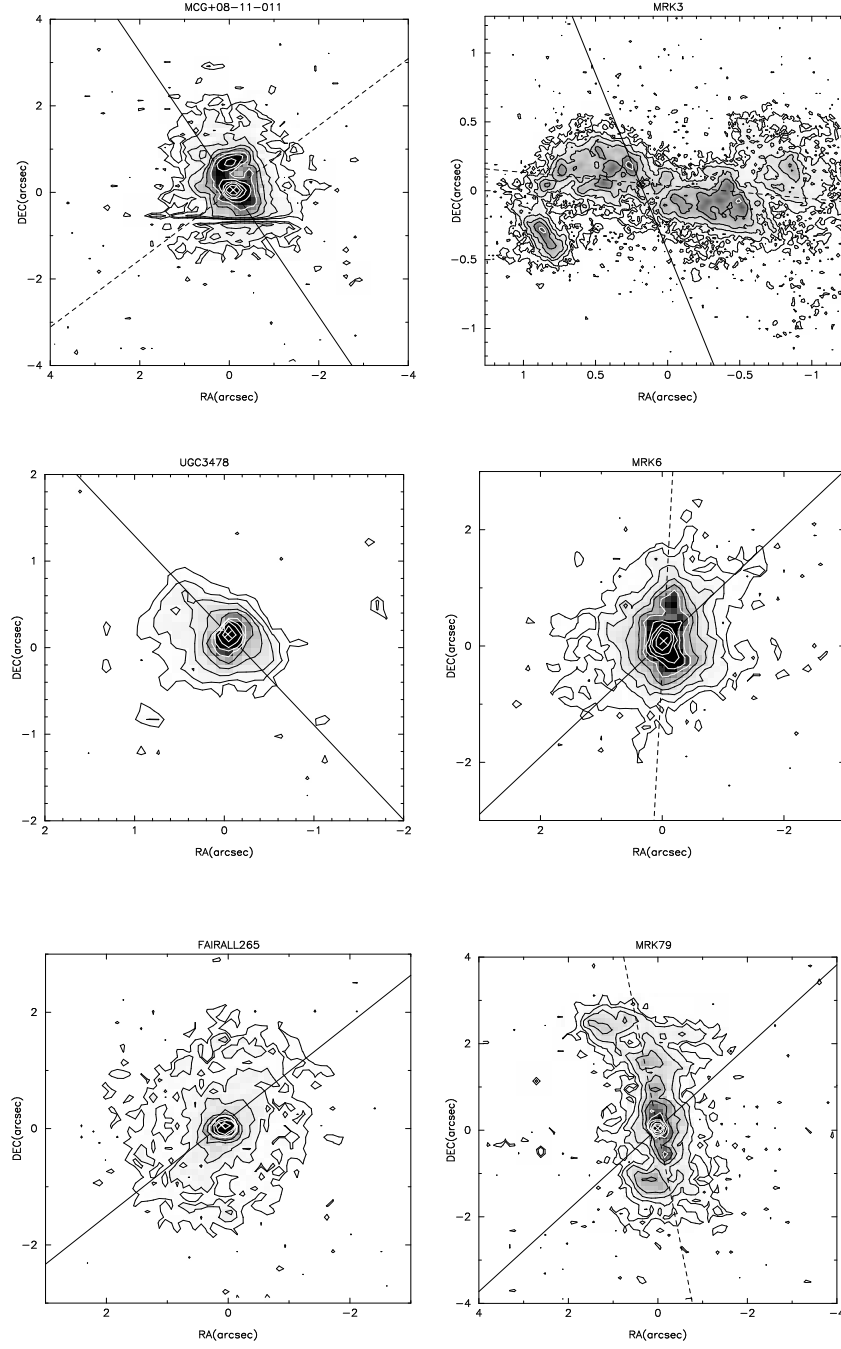


FIG. 8.— Same as Figure 5 for MCG +08-11-011, MRK 3, UGC 3478, MRK 6, Fairall 265 and MRK 79.

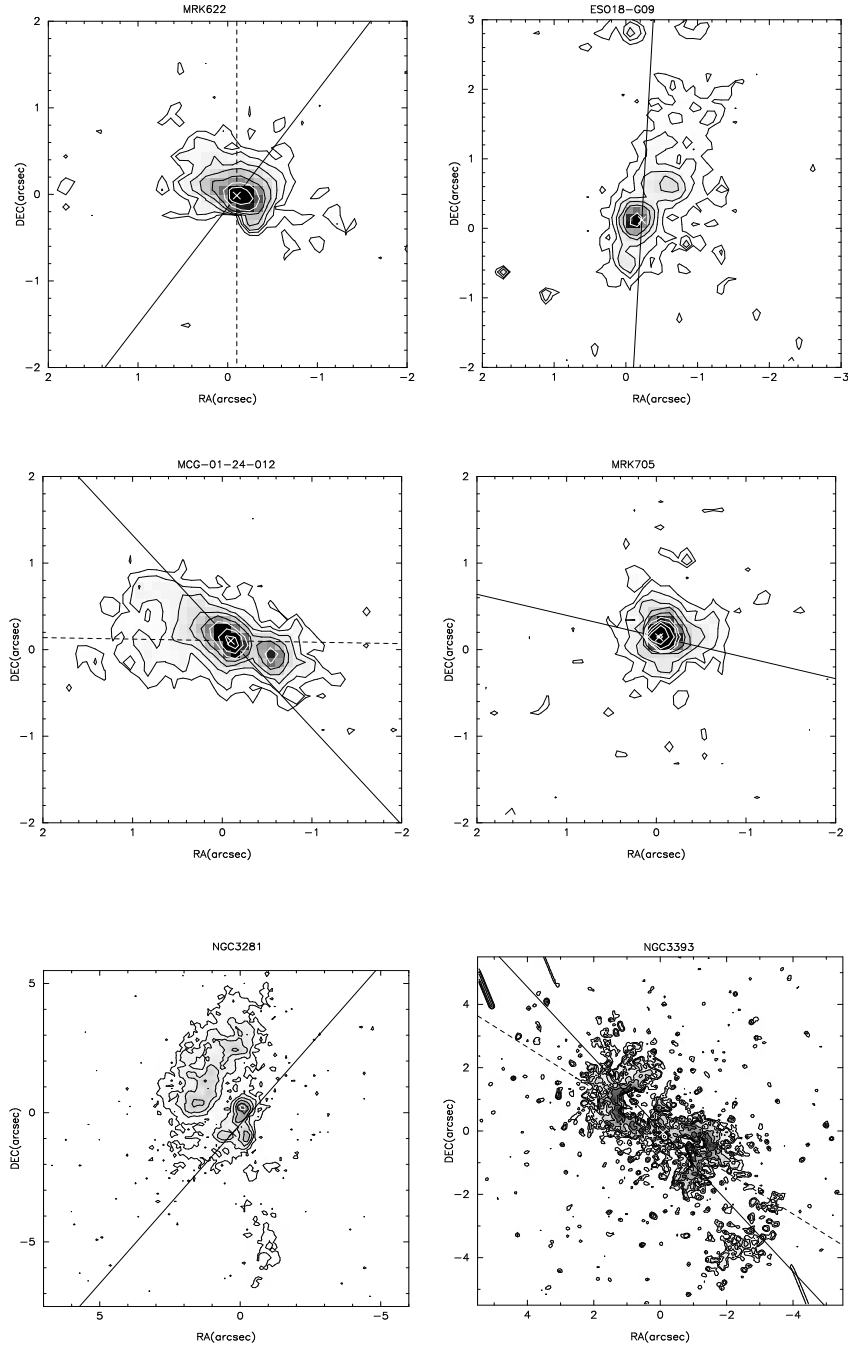


FIG. 9.— Same as Figure 5 for MRK 622, ESO 18-G 09, MCG -01-24-012, MRK 705, NGC 3281 and NGC 3393.

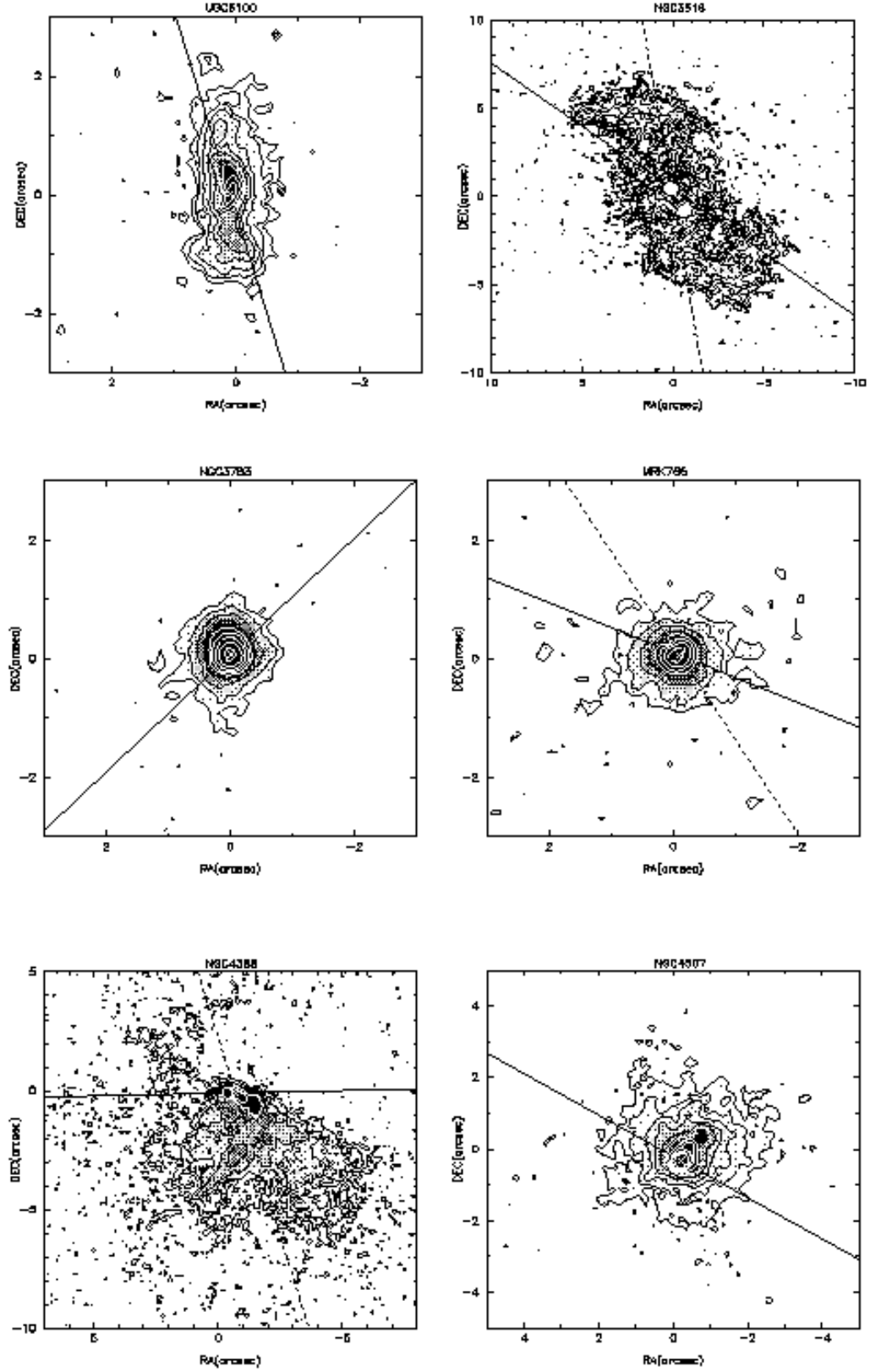


FIG. 10.— Same as Figure 5 for UGC 6100, NGC 3516, NGC 3783, MRK 766, NGC 4388 and NGC 4507.

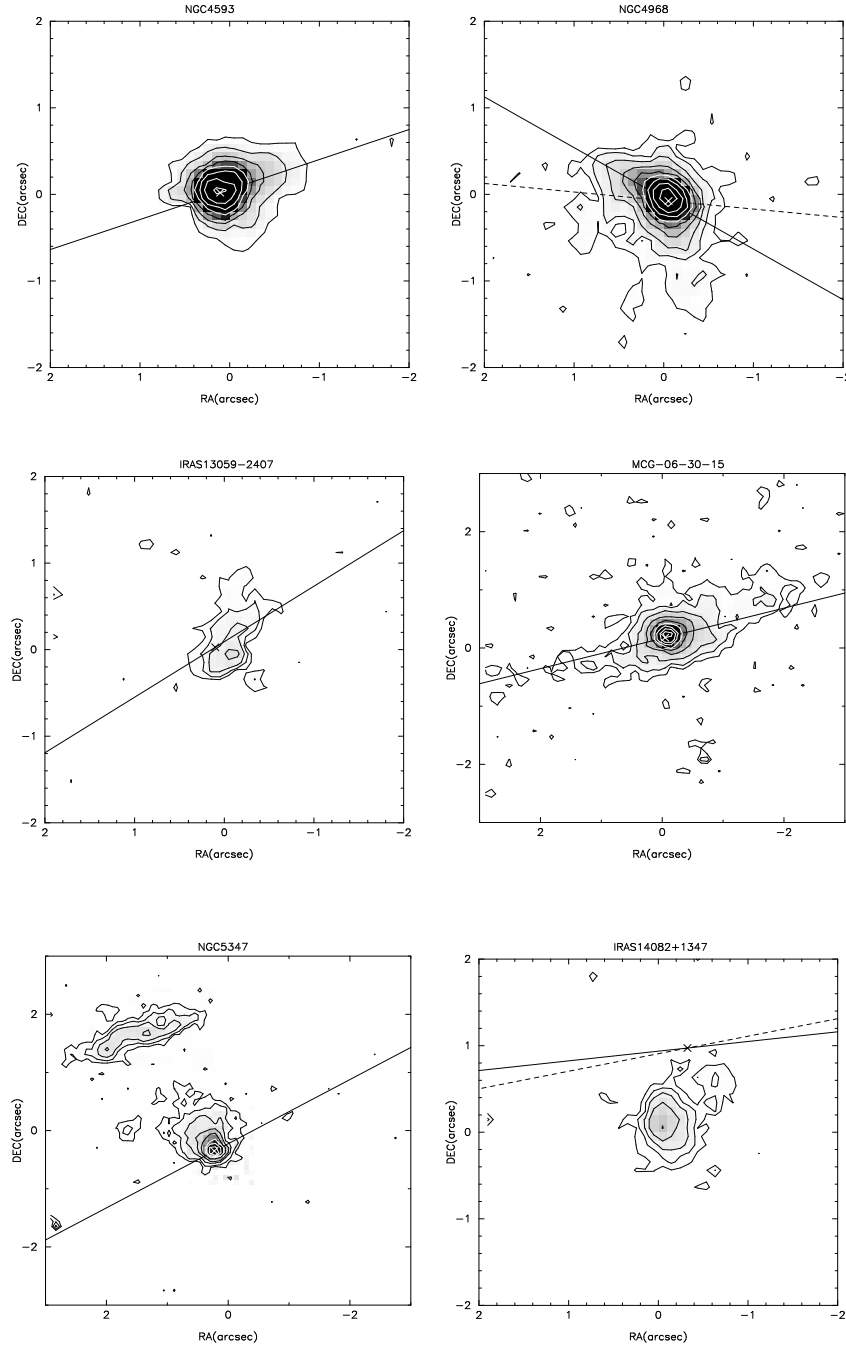


FIG. 11.— Same as Figure 5 for NGC 4593, NGC 4968, IRAS 13059-2407, MCG -6-30-15, NGC 5347, IRAS 14082+1347.

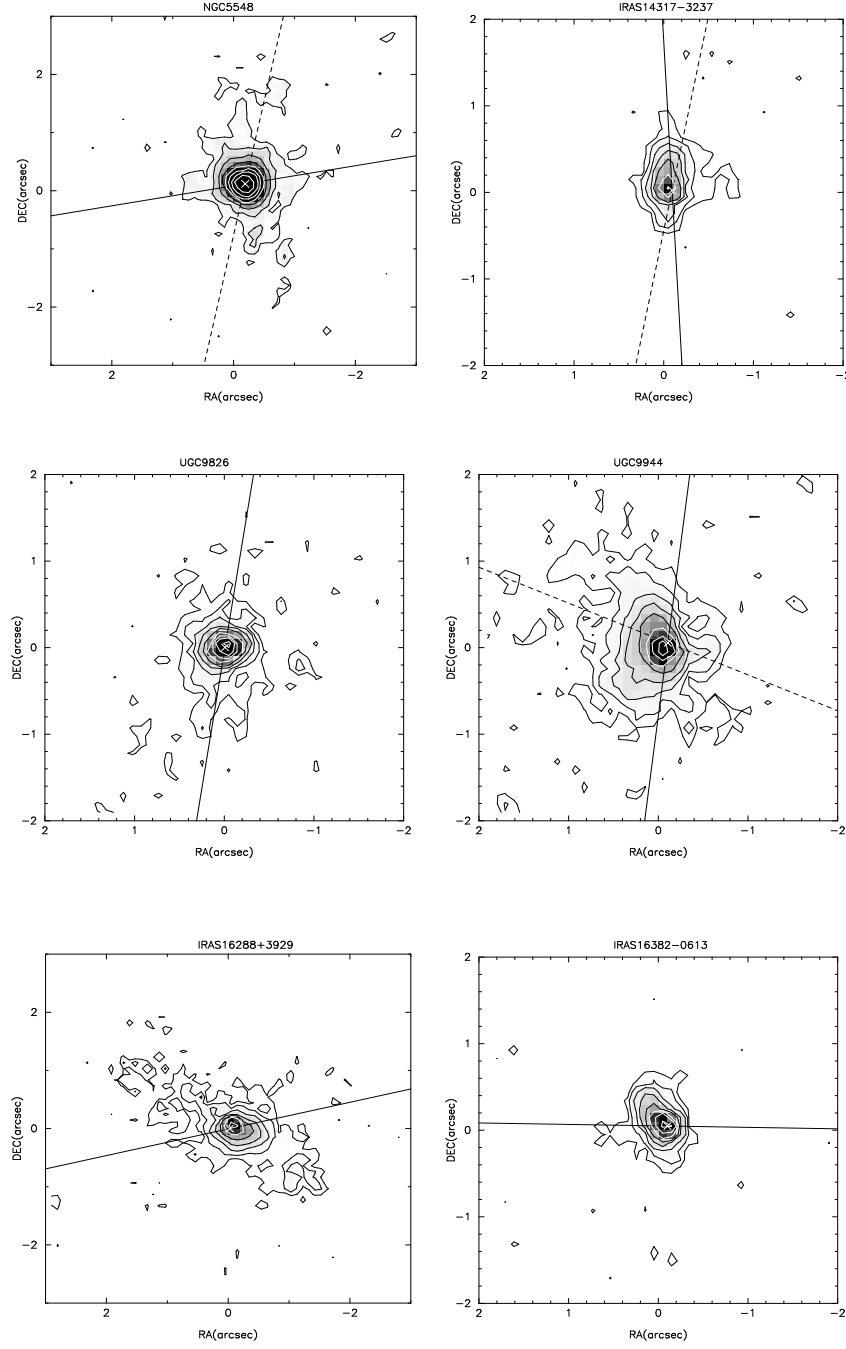


FIG. 12.— Same as Figure 5 for NGC 5548, IRAS 14317-3237, UGC 9826, UGC 9944, IRAS 16288+3929, IRAS 16382-0613.

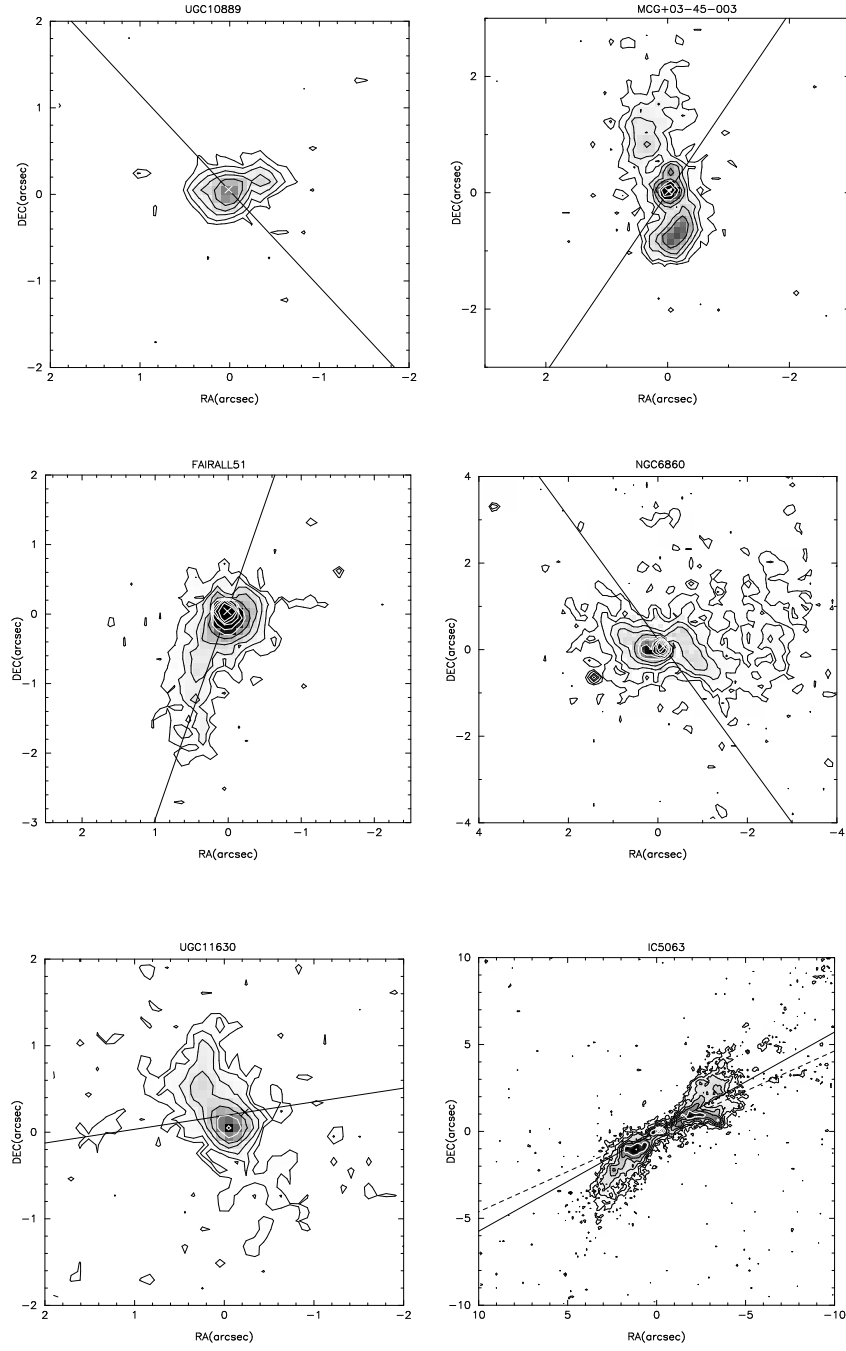


FIG. 13.— Same as Figure 5 for UGC 10889, MCG +03-34-003, Fairall 51, NGC 6860, UGC 11630, IC 5063.

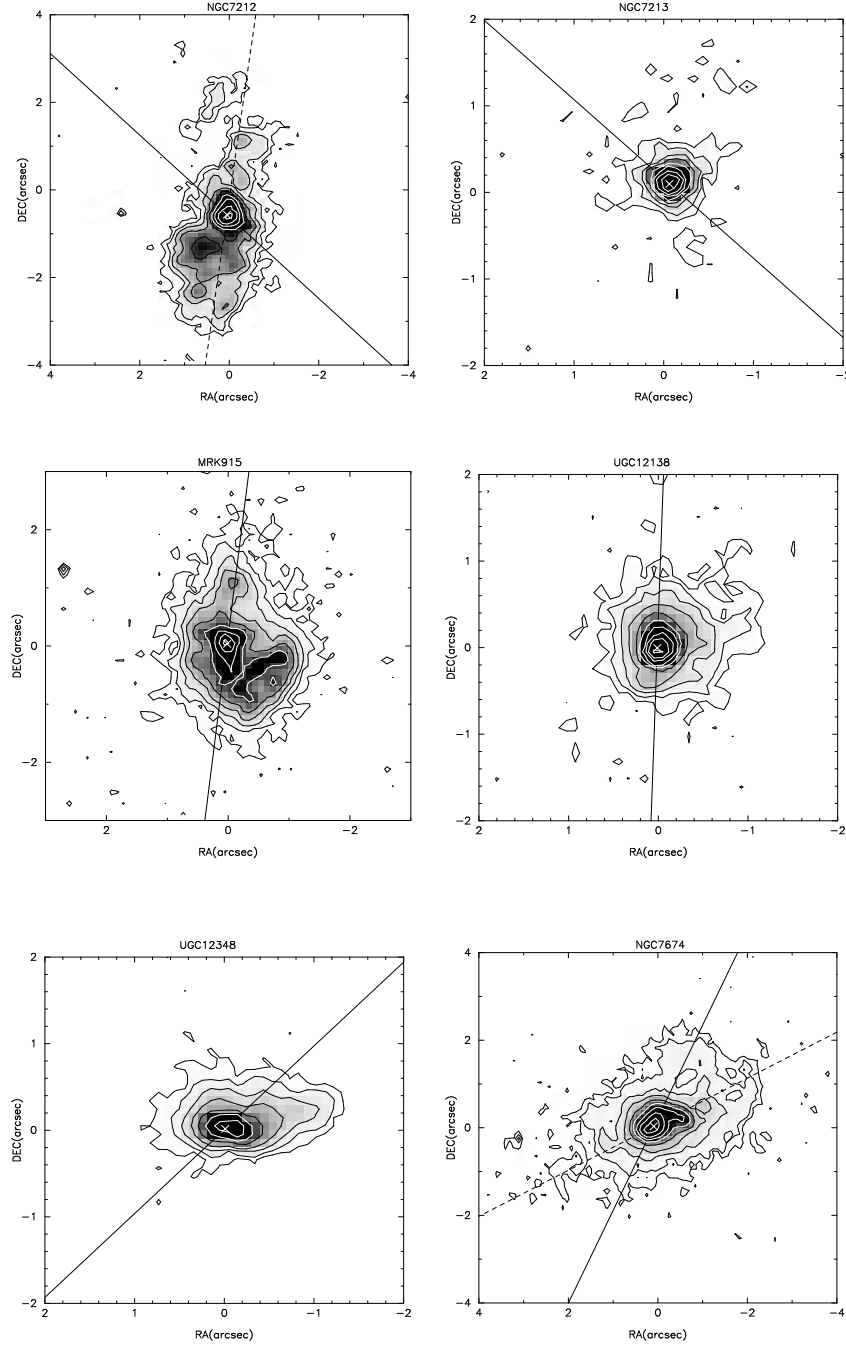


FIG. 14.— Same as Figure 5 for NGC 7212, NGC 7213, MRK 915, UGC 12138, UGC 12348, NGC 7674.

TABLE 1
OBSERVATIONS SUMMARY

Name (1)	RA (J2000) (2)	DEC (J2000) (3)	Exposure (seconds) (4)	Dataset Name (5)	Proposal (6)	Comments (7)
MRK 348	00 48 47.1	+31 57 25	600	U2XI0601T,U2XI0602T	6332	a
MRK 573	01 43 57.8	+02 21 00	280	U2XI0603T,U2XI0604T	6332	a
IRAS 01475-0740	01 50 02.7	-07 25 48	600	U2XI0701T,U2XI0702T		
ESO 153-G 20	02 06 03.6	-55 11 35	280	U2XI0703T,U2XI0704T	8598	
MRK 590	02 14 33.6	-00 46 00	800	U67L0301R,U67L0302R	8598	
MRK 1040	02 28 14.5	+31 18 42	80	U67L0303R	8598	
UGC 2024	02 33 01.2	+00 25 15	800	U67L0401R,U67L0402R	8598	
NGC 1068	02 42 40.7	-00 00 48	80	U67L0403R	8598	
MRK 1058	02 49 51.8	+34 59 17	800	U67L5801R,U67L5802R	8598	
MCG -02-08-039	03 00 29.8	-11 24 59	80	U67L5803R	8598	
UGC 2514	03 03 48.5	-01 06 13	800	U67L0501R,U67L0502R	8598	
IRAS 03106-0254	03 13 08.3	-02 43 19	80	U67L0503R	8598	
IRAS 03125+0119	03 15 05.3	+01 30 30	1000	U67L0701R,U67L0702R	8598	
MRK 607	03 24 48.7	-03 02 33	80	U67L0703R	8598	
ESO 116-G 18	03 24 53.1	-60 44 20	900	U2M30103T,U2M30104T	5754	b
NGC 1386	03 36 45.4	-35 59 57	440	U2M30101T,U2M30102T	8598	
ESO 33-G 02	04 55 59.6	-75 32 27	800	U67L5901R,U67L5902R	8598	
MCG -05-13-017	05 19 35.5	-32 39 30	80	U67L5903R	8598	
MCG +08-11-011	05 54 53.6	+46 26 22	600	U67L0801R,U67L0802R	8598	c
MRK 3	06 15 36.3	+71 02 15	80	U67L0803R	8598	
UGC 3478	06 32 47.3	+63 40 25	1000	U67L0901R,U67L0902M	8598	
MRK 6	06 52 12.3	+74 25 37	80	U67L0903R	8598	
FAIRALL 265	06 56 29.7	-65 33 43	1000	U67L1001R,U67L1002R	8598	
MRK 79	07 42 32.8	+49 48 35	80	U67L1003R	8598	
MRK 622	08 07 41.0	+39 00 15	800	U67L1101R,U67L1102R	8598	
ESO 18-G 09	08 24 07.4	-77 46 53	80	U67L1103R	8598	
MCG -01-24-012	09 20 51.7	-08 04 47	400	U3A00101T,U3A00102T	6419	
MRK 705	09 26 03.3	+12 44 04	80	U3A00103T,U3A00104T	8598	
NGC 3281	10 31 52.1	-34 51 13	800	U67L1201R,U67L1202R	8598	
NGC 3393	10 48 24.0	-25 09 40	80	U67L1203R	8598	
UGC 6100	11 01 34.0	+45 39 14	800	U3A00201M,U3A00202M	6419	b
NGC 3516	11 06 47.5	+72 34 07	80	U3A00203M,U3A00204M	8598	
IRAS 11215-2806	11 24 02.6	-28 23 15	800	U67L1501R,U67L1502R	8598	
NGC 3783	11 39 01.8	-37 44 20	80	U67L1503R	8598	
MRK 766	12 18 26.5	+29 48 46	600	U67L1601R,U67L1602R	8598	
NGC 4388	12 25 46.7	+12 39 41	80	U67L1603R	8598	
NGC 4507	12 35 37.0	-39 54 31	750	U67L6001R,U67L6002R	8598	
NGC 4593	12 39 39.4	-05 20 39	80	U67L6003R	8598	
			1196	X2580103T	5140	d
			1196	X2580104T	5140	d
			800	U67L1701R,U67L1702R	8598	
			80	U67L1703R	8598	
			600	U67L1801R,U67L1802R	8598	
			80	U67L1803R	8598	
			1000	U67L1901R,U67L1902R	8598	c
			80	U67L1903R	8598	
			600	U67L2001R,U67L2002R	8598	
			80	U67L2003R	8598	
			800	U67L2301R,U67L2302R	8598	
			80	U67L2303R	8598	
			1000	U67L2401R,U67L2402R	8598	
			80	U67L2403R	8598	
			800	U67L2501R,U67L2502R	8598	
			80	U67L2503R	8598	
			800	U67L6101N,U67L6102R	8598	c
			80	U67L6103R	8598	
			800	U67L6201R,U67L6202R	8598	
			80	U67L6203R	8598	
			10000	W1DB0405T,W1DB0406T,W1DB0407T	3982	e
				W1DB0408T,W1DB0409T		
			600	W1DB0401T		
			1000	U67L6301R,U67L6302R	8598	c
			80	U67L6303R	8598	
			1600	U3A00601T,U3A00602T	6419	
			140	U3A00603T,U3A00604T	8598	f
			1	U67L2601R,U67L2602R	8598	
			80	U67L2603R	8598	
			400	U5GU0105R,U5GU0106R	8240	g
				U5GU0107M,U5GU0108R		
			16	U5GU0103R,U5GU0104R	8240	g
			480	U5GU0205R,U5GU0206R	8240	
				U5GU0207R,U5GU0208R		
			20	U5GU0203R,U5GU0204R	8240	
			280	U2XI0201T,U2XI0202T	6332	a
			280	U2XI0203T,U2XI0204T	8259	g
			520	U5DF0105R,U5DF0106R	8259	g
			200	U5DF0101R,U5DF0102R	8240	g
			320	U5GU0306R,U5GU0307M	8240	g
				U5GU0308R,U5GU0309R		

TABLE 1—*Continued*

Name	RA (J2000)	DEC (J2000)	Exposure (seconds)	Dataset Name	Proposal	Comments
(1)	(2)	(3)	(4)	(5)	(6)	(7)
NGC 4968	13 07 07.6	-23 40 43	300 400 80	U5GU0305R U3A00801P,U3A00802P U3A00803P,U3A00804P	6419	
IRAS 13059-2407	13 08 42.1	-24 23 00	1000 80	U67L3401R,U67L3402R U67L3403R	8598	
MCG -6-30-15	13 35 53.7	-34 17 45	400 80	U3A00901T,U3A00902T U3A00903T,U3A00904T	6419	
NGC 5347	13 53 17.8	+33 29 27	800 80	U67L3701R,U67L3702R U67L3703R	8598	
IRAS 14082+1347	14 10 41.4	+13 33 29	1000 80	U67L3801R,U67L3802R U67L3803R	8598	
NGC 5548	14 17 59.5	+25 08 12	480 24	U5GU0505R,U5GU0506R U5GU0507R,U5GU0508R U5GU0503R,U5GU0504R	8240	g
IRAS 14317-3237	14 34 44.9	-32 50 28	1000 80	U67L3901R,U67L3902R U67L3903R	8598	
UGC 9826	15 21 33.0	+39 12 01	800 80	U67L4101R,U67L4102R U67L4103R	8598	c
UGC 9944	15 35 47.8	+73 27 02	800 80	U67L4201R,U67L4202R U67L4203R	8598	
IRAS 16288+3929	16 30 32.6	+39 23 03	800 80	U67L4401R,U67L4402R U67L4403R	8598	c
IRAS 16382-0613	16 40 52.3	-06 18 52	1000 80	U67L4501R,U67L4502R U67L4503R	8598	
UGC 10683 B	17 05 00.4	-01 32 29	1 80	U67L6501R,U67L6502R U67L6503R	8598	f
UGC 10889	17 30 20.7	+59 38 20	1000 80	U67L4601R,U67L4602R U67L4603R	8598	
MCG +03-45-003	17 35 32.7	+20 47 48	600 80	U67L7001R,U67L7002R U67L7003R	8598	
FAIRALL 49	18 36 58.1	-59 24 09	600 80	U67L4701R,U67L4702R U67L4703R	8598	h
FAIRALL 51	18 44 54.3	-62 21 49	600 80	U67L4801R,U67L4802R U67L4803R	8598	
NGC 6860	20 08 46.1	-61 05 56	1000 80	U67L4901R,U67L4902R U67L4903R	8598	
UGC 11630	20 47 33.5	+00 24 42	1000 80	U67L5101R,U67L5102R U67L5103M	8598	
IC 5063	20 52 02.0	-57 04 09	600 80	U67L5201M,U67L5202R U67L5203R	8598	
NGC 7212	22 07 02.0	+10 14 00	600 280	U2XI0401T,U2XI0402T U2XI0403T,U2XI0404T	6332	a
NGC 7213	22 09 16.2	-47 10 00	600 80	U67L5301R,U67L5302R U67L5303R	8598	
MRK 915	22 36 46.5	-12 32 45	600 80	U67L5401R,U67L5402R U67L5403R	8598	
UGC 12138	22 40 17.0	+08 03 14	600 80	U67L5501R,U67L5502R U67L5503R	8598	
UGC 12348	23 05 19.4	+00 11 28	600 80	U67L5701R,U67L5702R U67L5703R	8598	
NGC 7674	23 27 56.7	+08 46 45	520 200	U5DF0206R,U5DF0205R U5DF0201R,U5DF0202R	8259	i

^aOn-band and off-band images were obtained on different WF chips.

^bOn-band image obtained using the filter F502N, with the galaxy centered on the PC chip.

^cUsed a redshift slightly smaller than the observed one to force the galaxy to fall on the WF camera instead of the PC camera.

^dImages obtained with FOC camera.

^eImages obtained with the WF/PC1 in the PC mode, with the filter centered at [OIII] λ 4959Å.

^fObservation failed because of guide star acquisition problems.

^gOn-band observed with the WF and the off-band with the PC camera.

^hGalaxy located on a bad column on the CCD. Data lost.

ⁱObservations taken with the PC camera.

TABLE 2
SAMPLE CHARACTERISTICS

Name (1)	Alternative Name (2)	Type (3)	V_{Rad}^a (4)	$3\sigma^b$ (5)	$F([OIII])_{int}^c$ (6)	$F([OIII])_{nuc}^c$ (7)	$F([OIII])_{lit}^c$ (8)	$\log L([OIII])^d$ (9)	Ref. ^e (10)
MRK 348	NGC 262	2	4540	10.0	41.2	30.33	36.0	41.26	1
MRK 573	UGC 1214	2	5174	6.00	159.0	31.15	93.0	41.96	1
IRAS 01475-0740		2	5306	3.91	5.44	5.12	5.3	40.51	1
ESO 153-G 20	IRAS 02043-5525	2	5917	3.43	6.34	1.81	4.2	40.68	1
MRK 590	NGC 863	1	7910	3.51	13.6	11.29	5.3	41.26	2
MRK 1040	NGC 931	1	4927	4.10	10.9	8.98	7.5	40.75	1
UGC 2024		2	6714	3.00	5.50	2.24	2.5	40.72	1
NGC 1068		2	1136	2.75	1220.0	808.4	484.0	41.53	1
MRK 1058	IRAS 02467+3446	2	5138	3.97	5.49	2.47	5.6	40.49	2
MCG -02-08-039	IRAS 02580-1136	2	8874	4.60	19.5	13.40	18.0	41.51	1
UGC 2514	NGC 1194	1	3957	3.36	1.20	0.46	1.4	39.60	1
IRAS 03106-0254		2	8154	3.05	3.58	1.41	2.3	40.71	1
IRAS 03125+0119		2	7200	4.00	4.97	3.14	6.1	40.74	1
MRK 607	NGC 1320	2	2716	5.96	17.6	14.53	12.0	40.44	1
ESO 116-G 18	IRAS 03238-6054	2	5546	3.78	2.97	1.94	5.2	40.29	1
NGC 1386		2	868	4.38	51.4	38.62	80.0	39.92	2
ESO 33-G 02	IRAS 04575-7537	2	5426	3.85	6.21	4.13	5.7	40.59	1
MCG -05-13-017	IRAS 05177-3242	1	3790	4.47	30.7	26.51	34.0	40.97	1
MCG +08-11-011	UGC 3374	1	6141	3.26	64.3	34.23	71.0	41.71	2
MRK 3		2	4050	4.31	205.0	57.10	107.0	41.86	1
UGC 3478		1	3828	3.53	8.84	7.63	5.8	40.44	1
MRK 6	IC 450	1	5537	5.48	79.6	49.87	70.0	41.72	1
Fairall 265	IRAS 06563-6529	1	8844	4.51	18.3	9.17	2.8	41.48	1
MRK 79	UGC 3973	1	6652	3.94	40.6	19.16	37.0	41.58	2
MRK 622	UGC 4229	2	6964	3.95	5.08	2.85	4.0	40.72	2
ESO 18-G 09	IRAS 08255-7737	2	5341	3.18	4.21	1.91	3.2	40.41	1
MCG -01-24-012	IRAS 09182-0750	2	5892	3.42	7.16	3.77	8.9	40.72	1
MRK 705	UGC 5025	1	8658	4.06	12.4	9.69	9.0	41.30	2
NGC 3281		2	3200	4.10	25.0	1.61	5.5	40.74	2
NGC 3393		2	4107	2.38	105.0	5.97	99.0	41.58	1
UGC 6100		2	8778	3.59	20.5	7.13	28.0	41.53	3
NGC 3516		1	2649	1.94	69.3	23.47	35.0	41.02	1
NGC 3783		1	2550	16.5	86.3	81.63	76.0	41.08	1
MRK 766	NGC 4253	1	3876	10.5	39.5	31.55	45.0	41.10	1
NGC 4388		2	2524	7.87	134.0	21.55	66.0	41.26	1
NGC 4507		2	3538	4.26	110.0	78.29	83.0	41.47	1
NGC 4593		1	2698	13.6	22.9	21.80	13.0	40.55	1
NGC 4968	MCG -04-31-030	2	2957	5.77	20.4	18.55	18.0	40.58	1
IRAS 13059-2407		2	4175	2.97	0.63	0.37	1.2	39.37	1
MCG -6-30-15		1	2323	4.00	14.8	12.39	7.5	40.23	1
NGC 5347		2	2335	3.71	7.92	5.27	4.5	39.96	1
IRAS 14082+1347		2	4836	3.23	1.02	0.02	2.8	39.71	1
NGC 5548		1	5149	10.5	41.3	32.86	73.0	41.37	1
IRAS 14317-3237		2	7615	3.00	1.75	0.92	2.1	40.34	1
UGC 9826		1	8754	3.18	5.12	3.47	5.2	40.92	1
UGC 9944		2	7354	3.44	6.87	2.78	4.7	40.90	1
IRAS 16288+3929		2	9091	3.62	4.83	1.33	2.2	40.93	1
IRAS 16382-0613		2	8317	3.08	2.87	1.94	2.8	40.63	1
UGC 10889	NGC 6393	2	8424	2.82	1.38	0.65	2.2	40.32	1
MCG +03-45-003	IRAS 17334+2049	2	7292	4.70	9.58	2.91	26.0	41.04	1
Fairall 51	IRAS 18401-6225	1	4255	4.38	27.2	24.34	19.0	41.02	1
NGC 6860	ESO 143-G 09	1	4462	2.20	18.1	10.75	2.5	40.89	1
UGC 11630	NGC 6967	2	3657	3.20	3.18	1.68	2.6	39.96	1
IC 5063	PKS 2048-57	2	3402	4.04	77.2	9.95	56.0	41.28	1
NGC 7212		2	7984	13.8	87.5	21.28	70.0	42.08	2
NGC 7213		1	1792	10.0	13.6	13.09	13.0	39.97	1
MRK 915	IRAS 22340-1248	1	7230	5.17	47.3	9.53	31.0	41.72	1
UGC 12138		1	7375	5.37	21.9	14.68	14.0	41.40	1
UGC 12348		2	7585	6.47	10.1	4.22	13.0	41.09	1
NGC 7674	MRK 533	2	8713	3.22	52.1	12.03	52.1	41.93	1

^aThe units of Column (4) are km s^{-1} .

^bThe units of Column (5), the 3σ surface brightness level of the images, are $10^{-17} \text{ erg cm}^{-2} \text{ s}^{-1} \text{ pix}^{-1}$.

^cThe Units of Column (6), the integrated [OIII] flux, Column (7), the nuclear [OIII] flux, and Column (8), the [OIII] flux from the literature, are $10^{-14} \text{ erg cm}^{-2} \text{ s}^{-1}$.

^dThe units of Column (9), the integrated [OIII] luminosity are erg s^{-1} .

^eReferences for the [OIII] data from the literature: 1-) de Grijs et al. (1992); 2-) Whittle (1992); 3-) Cruz-Gonzalez et al. 1994.

TABLE 3
NLR SIZES

Name	R_e (pc)	R_{Maj} (pc)	R_{Min} (pc)	P.A. (°)	Offsets	Figure
(1)	(2)	(3)	(4)	(5)	(6)	(7)
MRK 348	56	420	255	185	0.16	5
MRK 573	505	1490	625	120	0.13	5
IRAS 01475-0740	33	145	130	—	0.00	5
ESO 153-G 20	163	505	355	-10 (-100)	0.43	5
MRK 590	49	385	280	-5	0.30	5
MRK 1040	40	240	175	45 (130)	0.00	5
UGC 2024	122	565	315	-35	0.10	6
NGC 1068	61	375	215	35	0.23	6
MRK 1058	123	380	235	205	0.56	6
MCG -02-08-039	75	630	530	—	0.08	6
UGC 2514	127	175	145	110	0.71	6
IRAS 03106-0254	119	395	235	30	0.33	6
IRAS 03125+0119	74	350	235	145	0.33	7
MRK 607	31	330	120	-45	0.44	7
ESO 116-G 18	66	305	180	75	0.56	7
NGC 1386	46	165	45	0	0.20	7
ESO 33-G 02	70	255	175	-5	0.09	7
MCG -05-13-017	32	250	190	-40	0.11	7
MCG +08-11-011	87	725	605	20	0.24	8
MRK 3	147	290	130	90	0.33	8
UGC 3478	32	205	145	55	0.09	8
MRK 6	68	575	390	-10	0.08	8
Fairall 265	100	985	830	-20	0.04	8
MRK 79	129	990	460	15	0.29	8
MRK 622	88	290	215	55	0.23	9
ESO 18-G 09	135	520	190	-30	0.37	9
MCG -01-24-012	93	440	220	75	0.09	9
MRK 705	62	350	280	—	0.22	9
NGC 3281	430	630	345	5 (50)	0.68	9
NGC 3393	446	705	370	65	0.01	9
UGC 6100	145	995	370	0	0.12	10
NGC 3516	361	1165	590	20	0.10	10
NGC 3783	31	175	140	-10	0.00	10
MRK 766	50	255	215	65	0.02	10
NGC 4388	385	635	500	90 (205)	0.80	10
NGC 4507	50	400	375	-35	0.30	10
NGC 4593	31	150	120	100	0.19	11
NGC 4968	31	210	125	40	0.14	11
IRAS 13059-2407	84	180	70	-20	0.47	11
MCG -6-30-15	27	295	115	-65	0.23	11
NGC 5347	39	235	185	30	0.78	11
IRAS 14082+1347	153	155	115	165	1.00	11
NGC 5548	57	450	350	5	0.09	12
IRAS 14317-3237	94	345	185	-5	0.29	12
UGC 9826	65	435	255	165	0.26	12
UGC 9944	128	475	355	0 (90)	0.07	12
IRAS 16288+3929	191	795	470	65	0.17	12
IRAS 16382-0613	70	325	240	15	0.15	12
UGC 10889	109	340	220	-85	0.18	13
MCG +03-45-003	269	705	300	15	0.25	13
Fairall 51	29	635	170	160 (210)	0.59	13
NGC 6860	62	650	345	85	0.19	13
UGC 11630	30	190	100	30	0.16	13
IC 5063	462	1320	330	-65	0.04	13
NGC 7212	225	1240	540	170	0.17	14
NGC 7213	14	65	65	—	0.13	14
MRK 915	280	955	610	5	0.08	14
UGC 12138	67	395	345	130	0.21	14
UGC 12348	123	540	280	100	0.23	14
NGC 7674	86	1240	760	120	0.25	14